JOURNAL OF GEOPHYSICAL RESEARCH, VOL. 101, NO. D16, PAGES 21,195–21,212, SEPTEMBER 27, 1996

An idealized ray model of gravity wave–tidal interactions

Stephen D. Eckermann[1]
Computational Physics, Inc., Fairfax, Virginia

Crispin J. Marks
National Institute of Water and Atmospheric Research Limited, Wellington, New Zealand

Abstract. The interaction of a gravity wave with a solar tide is analyzed using ray theory in order to assess whether the temporal oscillation of the tide has any significant effects on the interaction. We consider two types of solution: a "full ray solution," in which tidal accelerations are included in the gravity wave ray-tracing equations, and a second "Lindzen solution," in which they are neglected; the latter is so named because it yields similar results to the parameterization of *Lindzen* [1981]. Initially, we consider an idealized tide of constant velocity amplitude in a steady isothermal atmosphere, as this allows analytical solutions to be derived. A numerical ray-tracing code is employed to determine ray solutions within more complex tidal backgrounds. Full ray solutions often differ markedly in amplitude, wavenumber, and trajectory from Lindzen solutions for the same wave, highlighting the importance of tidal accelerations. Tidal accelerations have a stabilizing influence on gravity wave amplitudes by refracting waves to larger intrinsic phase speeds, thus reducing both the occurrence and intensity of tidally modulated gravity wave breaking. Even in the absence of dissipation, time-varying refraction gives rise to time-oscillating gravity wave action densities, $\partial A/\partial t$, which in turn lead to wave momentum-flux densities which are anticorrelated with tidal winds in agreement with mesospheric observations. Although $\partial A/\partial t$ averages to zero over one cycle of a constant-amplitude tide, its phase locking to the tide implies transient flow accelerations which temporarily amplify tidal wind oscillations and might permanently change tidal amplitudes in a nonlinear interactive model. Numerical simulations through more complex tidal backgrounds show instances where permanent $\partial A/\partial t$ values are induced in a gravity wave through its interaction with the tide. Our results point to weaknesses in a Lindzen parameterization of gravity wave–tidal interactions. A simple extension of the parameterization is suggested which incorporates some of these time-varying influences.

Introduction

Dissipation of gravity wave amplitudes in the atmosphere results in an *Eliassen and Palm* [1960] (EP) flux divergence which either accelerates or decelerates the local flow. In the middle atmosphere this wave driving of the flow tends to occur almost continuously, which maintains global flow patterns that differ substantially from a purely radiative circulation. The dissipated wave energy is transferred into turbulence which diffuses chemical species, which in turn influences the global and seasonal distributions of trace gases in the middle atmosphere.

Consequently, mean-flow accelerations and turbulent diffusion produced by dissipating gravity waves need to be incorporated accurately into global models of the middle atmosphere. *Lindzen* [1981] parameterized the physics of these processes by assuming a single linear saturated wave. His parameterization proved amenable to numerical implementation, and those models of the middle atmosphere which incorporated it often exhibited major improvements in their simulations [see, e.g., *Garcia and Solomon*, 1985; *Palmer et al.*, 1986]. These successes, along with its simplicity and general physical basis, quickly made it the standard way of incorporating gravity wave processes into large-scale models. Despite this, various shortcomings in the parameterization have been noted. These include its omission of localized turbulence effects [e.g., *Chao and Schoeberl*, 1984; *Coy and Fritts*, 1988; *Walterscheid and Schubert*, 1990], supersaturation [e.g., *Lindzen*, 1988; *McIntyre*, 1989], transience [e.g., *Fritts and Dunkerton*, 1984; *Walterscheid and Schubert*, 1990; *Laprise*, 1993], and various nonlinear and nonhydrostatic effects [e.g., *Fritts*, 1985; *Walterscheid and Schubert*, 1990; *Keller*, 1994].

Recently, parameterizations of a dissipating spectrum of gravity waves have been developed [*Fritts and Lu*, 1993; *Medvedev and Klaassen*, 1995]. While these spectra are more typical of the average wave energy distributions encountered in the middle atmosphere, individual wave events still often dominate the EP flux divergence in the stratosphere [e.g., *Bacmeister et al.*, 1994] and (less frequently) in the mesosphere [e.g., *Yamamoto et al.*, 1987; *Fritts et al.*, 1988]. Thus variants of the Lindzen scheme are still used commonly within middle atmosphere models to generate realistic diffusivities and circulation patterns [see, e.g., *Garcia and Boville*, 1994; *Jackson and Gray*, 1994; *Huang and Smith*, 1995; *Kinnersley*, 1996].

In the mesosphere the wave-breaking situation is further complicated by the presence of large-amplitude solar tides.

[1]Also at E. O. Hulburt Center for Space Research, Naval Research Laboratory, Washington, D. C.

Paper number 96JD01660.
0148-0227/96/96JD-01660$09.00

Report Documentation Page

Form Approved
OMB No. 0704-0188

1. REPORT DATE	2. REPORT TYPE	3. DATES COVERED
SEP 1996		**00-00-1996 to 00-00-1996**

4. TITLE AND SUBTITLE	5a. CONTRACT NUMBER
An idealized ray model of gravity wave-tidal interactions	5b. GRANT NUMBER
	5c. PROGRAM ELEMENT NUMBER
6. AUTHOR(S)	5d. PROJECT NUMBER
	5e. TASK NUMBER
	5f. WORK UNIT NUMBER
7. PERFORMING ORGANIZATION NAME(S) AND ADDRESS(ES) **Naval Research Laboratory,E.O. Hulburt Center for Space Research,Washington,DC,20375**	8. PERFORMING ORGANIZATION REPORT NUMBER
9. SPONSORING/MONITORING AGENCY NAME(S) AND ADDRESS(ES)	10. SPONSOR/MONITOR'S ACRONYM(S)
	11. SPONSOR/MONITOR'S REPORT NUMBER(S)

12. DISTRIBUTION/AVAILABILITY STATEMENT
Approved for public release; distribution unlimited

13. SUPPLEMENTARY NOTES

14. ABSTRACT
see report

15. SUBJECT TERMS

16. SECURITY CLASSIFICATION OF:			17. LIMITATION OF ABSTRACT	18. NUMBER OF PAGES	19a. NAME OF RESPONSIBLE PERSON
a. REPORT **unclassified**	b. ABSTRACT **unclassified**	c. THIS PAGE **unclassified**	**Same as Report (SAR)**	**18**	

Dissipation of tidal amplitudes can also produce significant mean-flow accelerations in the equatorial mesosphere and lower thermosphere [e.g., *Miyahara et al.*, 1993; *Hamilton*, 1995]. Furthermore, observations have revealed that large-amplitude tidal wind oscillations modulate gravity wave amplitudes and EP flux divergences [*Ganguly*, 1980; *Fritts and Vincent*, 1987; *Wang and Fritts*, 1991; *Thayaparan et al.*, 1995]. It is aspects of this latter process that we focus upon here.

The way in which gravity waves might interact with tides was explored initially by *Spizzichino* [1970] and *Walterscheid* [1981]. *Fritts and Vincent* [1987] applied a simple gravity wave saturation parameterization to model the interactions that they observed in radar winds, which revealed diurnally varying EP flux divergences in the presence of a diurnal tide. *Bjarnason et al.* [1987] also applied the Lindzen parameterization in a photochemical model to simulate tidally modulated diffusivities due to gravity wave breaking. These diurnally varying diffusivities in turn produced a diurnal variation in mesospheric ozone abundances which agreed well with observations. Later studies using the Lindzen parameterization illustrated that the mere presence of tides significantly altered even the daily averaged mean-flow accelerations and diffusivities produced by gravity wave breaking [*Hunt*, 1986, 1990; *McLandress and Ward*, 1994].

Fritts and Vincent [1987] also modeled the effect that tidally modulated gravity wave dissipation might have upon the tide itself. Reduced tidal amplitudes and an advancement of tidal phase in time were predicted. A similar gravity-wave-induced damping of mesospheric Rossby waves was postulated by *Lindzen* [1984] and *Schoeberl and Strobel* [1984] and later simulated in a model by *Miyahara* [1985] using the Lindzen parameterization (see also *Miyahara et al.* [1986]). Tidal modelers have used Lindzen-like parameterizations to examine the effects of gravity wave dissipation on global tidal structures [e.g., *Forbes et al.*, 1991; *McLandress and Ward*, 1994]. *Lu and Fritts* [1993] used a spectral parameterization to assess the effects (see also *Roble and Ridley* [1994]): They too found advances in tidal phase but noted that increases and decreases in tidal amplitudes were possible within their model. Progress in the modeling of these interactions has been reviewed by *Miyahara and Forbes* [1994], *Fritts* [1995], and *Walterscheid* [1995].

Use of the Lindzen parameterization in the presence of a tide requires that the tidal oscillation, as "seen" by a gravity wave, can be validly approximated as vertically varying but time-independent, so that conventional nontransient wave formulae can be used to describe the propagation and amplitude of any gravity wave through the tide [e.g., *Lindzen*, 1981]. This implies that the tidal phase and group speeds must be much slower than the group velocity of the gravity wave. Here we assess the accuracy of these assumptions by computing gravity wave trajectories in the presence of tides using ray techniques. We use ray-tracing equations appropriate for nonhydrostatic gravity waves, as given by *Marks and Eckermann* [1995], which we extend here to incorporate the refractive effects of tidal winds which oscillate both spatially and temporally. Throughout this study we simplify the assumed mean and tidal background wherever possible in order to focus on the essence of the gravity wave response within these tidal wind fields.

In drafting this manuscript the results of a similarly motivated ray-tracing study by *Zhong et al.* [1995] came to our attention. Their numerical simulations showed that time-varying tidal oscillations produced important refractive effects on gravity wave trajectories, as we have also found. Given this, we have changed the focus of this paper somewhat to concentrate less on ray trajectories (many examples of which are given by *Zhong et al.* [1995]) and more on the effects on gravity wave amplitudes and gravity wave–tidal interactions, which *Zhong et al.* [1995] did not simulate. Additionally, we have attempted to present a simple physical picture of the processes which operate here by deriving analytical solutions for a gravity wave in the presence of an idealized tidal wave of constant amplitude, drawing on studies of related phenomena in the ocean. In this way, comparisons among these results and those from simpler nontransient wave formulae, such as the Lindzen parameterization, are more easily made.

Simplified Ray-Tracing Model

We employ ray techniques to model gravity wave (GW) propagation through a prescribed tidal oscillation. General simulations of this kind can be performed accurately with the Gravity-wave Regional or Global Ray Tracer (GROGRAT), the first version of which (V1.0) was described by *Marks and Eckermann* [1995]. GROGRAT is a general numerical algorithm which simulates gravity wave propagation through an arbitrary atmosphere using ray-tracing methods. We are presently engaged in a major upgrade of GROGRAT to "next-generation" status (V2.0 and beyond). One purpose of this upgrade is to include time variations of the background atmosphere realistically into the model, to complement the three-dimensional spatial variations which are already catered for. The present study provides a simplified platform for developing and testing time-varying ray equations, while simultaneously providing useful insights into a specific phenomenon of considerable current interest in the middle and upper atmosphere.

While general numerical ray-tracing models like GROGRAT and others [e.g., *Zhong et al.*, 1995] give accurate solutions, they arrive at these solutions by numerically accumulating influences from a range of background parameters and all of their spatiotemporal derivatives. Thus it is not always easy to identify and separate the major dynamical interactions from a host of other minor contributions to these ray solutions, yet this is important in potentially refining the simple parameterizations of these processes used in larger-scale models. Thus to aid theoretical interpretation, we shall use a "stripped-down" version of the GROGRAT ray-tracing code, in which we retain only those processes which are essential to a first-order description of the GW-tidal interaction.

Ray Equations

The ray equations used here are as given in Appendix A of *Marks and Eckermann* [1995]. For example, refraction of the vertical wavenumber m is given by the ray-tracing equation

$$\frac{dm}{dt} = -kU_z - lV_z - \frac{1}{2\omega^+\Delta} \cdot [(N^2)_z(k^2 + l^2) - (\alpha^2)_z(\omega^{+2} - f^2)], \quad (1)$$

which replicates equation (A3f) of *Marks and Eckermann* [1995] and uses identical notation: $\boldsymbol{\kappa} = (k, l, m)$ is the wavenumber vector, $\omega^+ = \omega - \boldsymbol{\kappa} \cdot \mathbf{U}$ is the intrinsic frequency, and $\mathbf{U}$ is the background flow velocity, currently given an assumed horizontal form $(U, V, 0)$. Additional background variables are the Brunt-Väisälä frequency N, the Coriolis parameter f, and $\alpha = 1/2H_\rho$, where H_ρ is the density scale height. The time derivative in the ray-following frame is d/dt,

while subscripts denote partial derivatives in the Earth-based frame (i.e., $U_z = \partial U/\partial z$), and $\Delta = k^2 + l^2 + m^2 + \alpha^2$.

When local time variations of these background quantities (e.g., $U_t = \partial U/\partial t$) are ignored, the ground-based wave frequency ω remains constant along the ray ($d\omega/dt = 0$) [see, e.g., *Lindzen*, 1981; *Marks and Eckermann*, 1995]. However, a time-varying background atmosphere due to the presence of tides results in an additional ray-tracing equation [e.g., *Jones*, 1969; *Whitham*, 1974]

$$\frac{d\omega}{dt} = kU_t + lV_t + \frac{1}{2\omega^{+}\Delta}\left[(N^2)_t(k^2 + l^2) - (\alpha^2)_t(\omega^{+2} - f^2)\right]. \tag{2}$$

Thus $d\omega/dt \neq 0$ in general, and ω is no longer constant along the ray path.

Use of ray methods to specify gravity wave paths requires that the background atmosphere varies slowly compared to the wave oscillation, so that the (WKB) assumption of a single slowly modulated wave packet remains valid. Thus following *Marks and Eckermann* [1995] (see also *Broutman* [1984]), we first require that

$$\delta = \frac{1}{m^2}\left|\frac{\partial m}{\partial z}\right| \ll 1. \tag{3}$$

Since we evaluate $\partial m/\partial z$ directly in this study, as described in Appendix A, then the along-ray calculation used by *Marks and Eckermann* [1995] to approximate (3) is not needed here. *Zhong et al.* [1995] used the more formal WKB parameter of *Einaudi and Hines* [1970],

$$\tilde{\delta}^2 = Q_1 + Q_2 \ll 1, \tag{4}$$

where $Q_1 = -0.75m^{-4}(\partial m/\partial z)^2$ and $Q_2 = 0.5m^{-3}\,\partial^2 m/\partial z^2$. While Q_1 resembles δ^2 in (3), Q_2 is an additional higher-order term. *Zhong et al.* [1995] found that Q_2 was nonnegligible in their simulations, thus implying that the ray method of solution may be questionable in many circumstances. We estimated Q_2 in several similar simulations by subtracting $\partial m/\partial z$ at adjacent heights along the ray path to estimate an approximate $\partial^2 m/\partial z^2$ value and also found that nonnegligible Q_2 values sometimes arose.

There are two points worth noting about using along-ray calculations of (4) to gauge the applicability of the ray method. First, the extra terms in (4) account for possible partial reflection of wave energy due to sudden changes in the "refractive index" for the waves [see, e.g., *Blumen*, 1985]. Significant partial reflection of wave energy does not necessarily invalidate the use of ray methods to continue tracking the transmitted wave energy (although energy correction terms should obviously be included). A second point is that evaluating Q_2 by differencing adjacent points along the ray path does not give exact vertical partial derivatives, since such a calculation implicitly includes horizontal and time variations in m as well (assuming a generally oblique, time-varying ray path). As mentioned in Appendix A, accurate calculations of spatiotemporal partial derivatives of wave parameters at various points along the ray path generally require some sort of "ray tube" technique, in which the parameters of a number of closely spaced rays are interpolated to form a "tube," from which these derivatives can be inferred numerically [e.g., *Marks and Eckermann*, 1995]. So as not to complicate things unnecessarily in this study, we use (3) as our guide (as in section 5 of *Einaudi and Hines* [1970]) but ensure that our calculations obey the inequalities required of both our exact calculation of (3) and our approximate calculation of (4).

Our provision for a time-varying background atmosphere means that we must also satisfy slowly varying requirements in the time domain, which yields the following temporal analogue of (3) [e.g., *Broutman*, 1984]:

$$\gamma = \frac{1}{\omega^{+2}}\left|\frac{\partial \omega^{+}}{\partial t}\right| \ll 1. \tag{5}$$

Note that there is no temporal analogue of the *Einaudi and Hines* [1970] WKB derivation which led to (4). Equation (5) can also be evaluated exactly using $\partial m/\partial z$ values, as shown in Appendix A.

Simplified Mean and Tidal Background

In order to study the essence of the GW-tidal interaction we consider an idealized zonal wind field of the form

$$U(x, z, t) = U_{\mathrm{TIDE}}(z)\,\sin(Kx + Mz + n\Omega t + \varphi),$$
$$= U'_{\mathrm{TIDE}}(x, z, t), \tag{6}$$

where $K = n/(a\cos\theta)$ is the tidal horizontal wavenumber (a is the Earth's radius, θ is latitude, and n is a positive integer), M is the tidal vertical wavenumber, and $\Omega = 2\pi\,(24\ \mathrm{hours})^{-1}$. Thus the flow is produced by a purely zonal tidal wind oscillation of peak amplitude $U_{\mathrm{TIDE}}(z)$.

We take the background density ρ_0 at $z = 60$ km to be 3×10^{-4} kg m^{-3} and adopt a steady isothermal background temperature $\bar{T} = 240$ K, following *McLandress and Ward* [1994]. Variations in $\bar{T}$ (and hence N and α) can be large at the equator, where they make important contributions to gravity wave–tidal interactions [e.g., *Miyahara and Forbes*, 1994]. However, comparisons of isothermal and anisothermal extratropical simulations by *Zhong et al.* [1995] usually revealed small differences in ray trajectories, so we omit such effects here for simplicity and clarity of subsequent interpretation. One should note, however, that these and other parameter dependences (e.g., mean wind variations) can be accurately gauged using GROGRAT in the presence of more complicated background atmospheres.

For the simplified flow (6) then, since K is wavenumber-n (i.e., of planetary scale), $U_x = \partial U/\partial x$ is small, so k remains nearly constant, while l is refracted only slightly due to the latitudinal variation of f [e.g., *Dunkerton*, 1984; *Marks and Eckermann*, 1995]. Thus $\kappa_h = (k^2 + l^2)^{1/2}$ remains constant with height to a very good approximation when tracing any small-scale gravity wave through these tidal winds.

Consequently, to simplify things further in this study, we have set $K = 0$ in all the simulations to be reported here, so that the flow becomes

$$U(z, t) = U_{\mathrm{TIDE}}(z)\,\sin(Mz + n\Omega t + \varphi),$$
$$= U'_{\mathrm{TIDE}}(z, t). \tag{7}$$

We have conducted simulations with and without the Kx term in (6) and have found only small differences in the solutions when the waves do not propagate over long horizontal distances. The neglect of horizontal tidal variations is also addressed more formally in deriving analytical solutions for a constant tidal amplitude in the following section.

An advantage of using (7) is that it permits direct comparisons of our results with those of earlier studies, which used

zonal flow fields identical to (7) but did not incorporate the effects of time-varying tidal winds on the gravity wave equations [e.g., *Walterscheid*, 1981; *Lu and Fritts*, 1993; *McLandress and Ward*, 1994]. Thus any differences which arise can now be directly ascribed to time-varying tidal effects acting on the gravity wave. Another advantage is that the dependence of the flow on z and t alone allows accurate determinations of gravity wave amplitudes to be made along the ray, as described in the following section.

Gravity Wave Amplitudes

By far the greatest difficulty involved in including background time variations into a ray-tracing approach involves the accurate calculation of wave amplitudes along the ray path. A solution to the wave-action continuity relation

$$\frac{\partial A}{\partial t} + \nabla \cdot (\mathbf{c}_g A) = -\frac{2A}{\tau} \tag{8}$$

is required [*Bretherton and Garrett*, 1969], where A is the action density, $\mathbf{c}_g = (c_{gx}, c_{gy}, c_{gz})$ is the ground-based group velocity vector, and τ^{-1} is a damping term. Within the simplified background environments that we have just introduced, horizontal gradients of the horizontal action flux terms in (8) disappear, so that (8) can be simplified and reexpressed as

$$\frac{dA}{dt} = -A\left(\frac{\partial c_{gz}}{\partial z} + 2\tau^{-1}\right), \tag{9}$$

where $c_{gz} = dz/dt = \partial\omega/\partial m$. Again, $\partial c_{gz}/\partial z$ in (9) can be evaluated generally using a ray tube calculation. However, within the restricted backgrounds considered here, and on manipulating the equations, this term can be evaluated accurately along single ray paths using a ray equation for $\partial m/\partial z$ and given a sufficiently accurate initial condition. The method is outlined in Appendix A and is used in this model.

The damping rate τ^{-1} in GROGRAT parameterizes the effects of background turbulence and radiative damping on wave amplitudes [see *Marks and Eckermann*, 1995, Appendix B], but in the interests of simplicity we omit such influences here. However, we must include wave-breaking effects in some way. To compare as closely as possible with the Lindzen scheme, we replace the nonhydrostatic saturation scheme used in GROGRAT with the simpler static-instability saturation limit used by *Lindzen* [1981], which yields $a_{sat} = 1$ using the nomenclature of *Marks and Eckermann* [1995]. The saturated wave-action density then becomes [*Marks and Eckermann*, 1995]

$$A_{sat} = \frac{1}{4}\frac{\rho_0(z)\omega^4}{(k^2+l^2)}\left[1 + \frac{f^2}{\omega^{+2}} + \frac{N^2+\omega^{+2}}{N^2-\omega^{+2}}\left(1 - \frac{f^2}{\omega^{+2}}\right)\right]. \tag{10}$$

Thus whenever $A > A_{sat}$, action density is dissipated by inserting a damping factor $\tau = \tau_{sat}$ into (9) which returns the wave to marginal stability ($A = A_{sat}$).

Types of Solution

In what follows we shall consider two main solutions. The first is the solution produced using the ray methods just described and will be referred to as the full ray solution.

The second is calculated by keeping ω constant ($d\omega/dt = 0$), whereupon m simply follows from the dispersion relation

$$m^2 = \kappa_h^2 \frac{N^2-\omega^{+2}}{\omega^{+2}-f^2} - \alpha^2. \tag{11}$$

Group velocities are evaluated from these wave parameters and are used to define the ray's trajectory in this solution. Wave amplitudes are calculated by solving the wave-action equation in the absence of time variations, which yields the solution

$$Ac_{gz} = \text{const.} \tag{12}$$

This second ray solution gives results which are similar in many respects to the parameterization formulae of *Lindzen* [1981], as *Schoeberl* [1985] demonstrated. Hence we shall refer to them as "Lindzen solutions," although one should bear in mind that the correspondence is not exact. For example, the nonhydrostatic dispersion relation (11) represents a slight extension of the hydrostatic Lindzen theory.

In a steady environment with purely vertical background wind variations the full ray solution and the Lindzen solution give identical results. A major goal of this study is to assess whether the differences between the two solutions that arise on adding time variations to the background are significant. We shall focus most closely on any differences in wave amplitudes and the predicted amounts and locations of wave breaking.

Analytical Ray Solutions for Constant Tidal Amplitude

We consider first the simplest case of $U_{TIDE}(z)$ equal to a constant, $\hat{U}_{TIDE}$, in (6). In this case the ray and amplitude equations for the gravity wave can be solved analytically. Solutions to a somewhat similar oceanic problem were derived by *Thorpe* [1989] and tested using tank experiments.

The geometry of this problem is depicted in Figure 1. It shows a larger-scale gravity wave (in our case, a solar tide) of constant velocity amplitude propagating to the right, with phase moving down ($C_z < 0$) and energy moving upward ($C_{gz} > 0$). We assume a transverse wave with nonzero K, so we must also incorporate a vertical tidal velocity perturbation W' (see Figure 1). A smaller-scale gravity wave impinges upon the larger-scale wave oscillation from the bottom left. Assuming both waves are aligned east-west, then from (8) the action density A of the small-scale wave must obey the continuity relation

$$\frac{\partial A}{\partial t} + \frac{\partial}{\partial x}(c_{gx}A) + \frac{\partial}{\partial z}(c_{gz}A) = 0, \tag{13}$$

in the absence of dissipation. All three terms in (13) are clearly nonzero on inspecting Figure 1. However, on rotating the axes through an angle $\beta = \arctan(-K/M)$, such that the new axes x' and z' are aligned parallel and orthogonal, respectively, to the phase fronts of the tidal oscillation (see Figure 1), then (13) transforms and simplifies to

$$\frac{\partial A}{\partial t} + \frac{\partial}{\partial z'}(c_{gz'}A) = 0, \tag{14}$$

where $c_{gz'} = c_{gz}\cos\beta - c_{gx}\sin\beta$ is the gravity-wave group velocity along z'. The derivation of (14) follows from the invariance of A under Galilean transformations [e.g., *Grimshaw*, 1984] and since $\partial/\partial x'\,(c_{gx'}A) = 0$, as can be noted on inspecting Figure 1.

Finally, we transform to a third nonaccelerated frame with

axes (x'', z''). These axes have the same tilted orientation as the (x', z') axes in Figure 1 but move downward along the z' axis at the tidal phase speed, so that $x'' = x'$ and $z'' = z' - C_{z'}t$, where $C_{z'} = -|\mathbf{C}|$ (see Figure 1). Then (14) transforms and simplifies to

$$\frac{\partial}{\partial z''}(c_{gz''}A) = 0, \tag{15}$$

since tidal time variations disappear in this frame (i.e., $\partial A/\partial t = 0$). Equation (15) has the solution

$$c_{gz''}A = [(c_{gz}\cos\beta - c_{gx}\sin\beta) - C_{z'}]\,A = \text{const}, \tag{16}$$

where $C_{z'} = n\Omega/\mathcal{K}$, and $\mathcal{K} = (K^2 + M^2)^{1/2}$. Note that $c_{gz} = W' + c_{gz}^{\perp}$ and $c_{gx} = U' + c_{gx}^{+}$, where (c_{gx}^{+}, c_{gz}^{+}) is the intrinsic group velocity. However, since $W'\cos\beta - U'\sin\beta = 0$ (see Figure 1), then (16) can also be expressed as

$$\{(c_{gz}^{\perp}\cos\beta - c_{gx}^{-}\sin\beta) - C_{z'}\}\,A = \text{const}, \tag{17}$$

This same transformation sequence also simplifies the ray-tracing equations of the small-scale wave, such that in the frame (x'', z'') the observed frequency ω'' and wavenumber component along x'', denoted k'', remain constant. The following Doppler relations hold among the frequencies of the small-scale gravity wave measured from these different reference frames:

$$\omega = \omega' = \omega'' + C_{z'}m',$$

$$= \omega'' + C_{z'}(m\cos\beta - k\sin\beta). \tag{18}$$

Since $K^2 \ll M^2$ for solar tides, then $\beta = \arctan(-K/M)$ is very small and the rotational transformation $(x, z) \rightarrow (x', z')$ produces a very small effect in this problem. This implies that the tidal gradients along the x axis are small and have little influence on the ray path and amplitude of the small-scale gravity wave.

Thus we omit these effects by setting $\beta = 0$, just as we did earlier when setting $K = 0$ in going from (6) to (7) and assuming $W' = 0$. This simplifies the transformation sequence to a single transformation from (x, z) to (x'', z''), such that $z'' = z - C_z t$, $x'' = x$, and the axes (x'', z'') move downward with the vertical phase velocity of the tide $C_z = n\Omega/M$. The solutions now simplify to those derived and analyzed by *Broutman and Young* [1986] in their analysis of an oceanic gravity wave propagating through an inertial oscillation. Again, the wave frequency as measured from the frame (x'', z'') remains constant, so that from (18), $\beta = 0$ yields

$$\omega'' = \omega - C_z m = \text{const}. \tag{19}$$

Thus the ground-based frequency ω is periodically refracted as the tide oscillates temporally, according to (19), which is the solution of (2) for this problem. The remaining wave parameters vary so as to maintain the dispersion relation

$$\omega^{+2} = [\omega'' + C_z m - k\,U(z, t)]^2$$

$$= \frac{(k^2 + l^2)N^2 + (m^2 + \alpha^2)f^2}{\Delta}. \tag{20}$$

Using (16) with $\beta = 0$, the wave-action solution now simplifies to [*Broutman and Young*, 1986]

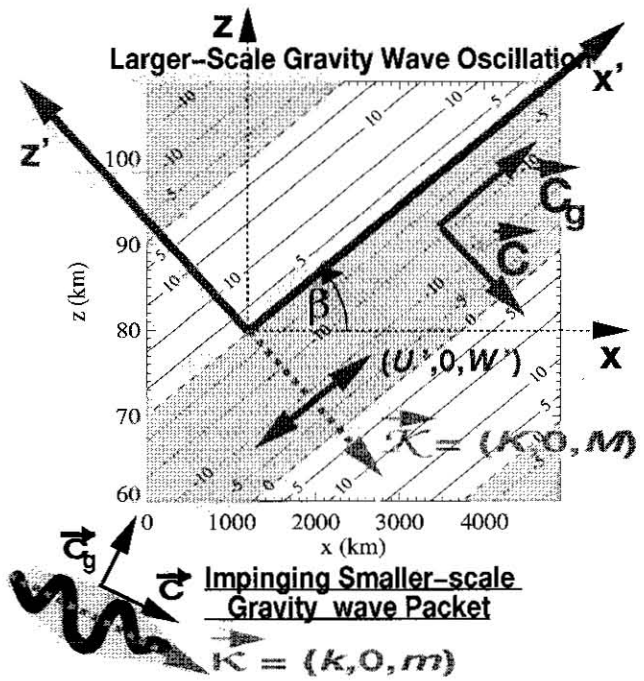

Figure 1. The contour plot depicts the velocity oscillations of a large-scale gravity wave with a peak velocity amplitude of 11 m s^{-1} (contour labels are in meters per second and negative values are shaded). The wavenumber vector $\mathcal{K}$, velocity oscillation vector $(U', 0, W')$, group velocity $\mathbf{C}_g$, and phase velocity $\mathbf{C}$ for this wave are also depicted. A smaller-scale gravity wave of wavenumber $\boldsymbol{\kappa}$ impinges on the big wave from the bottom left, with phase and group velocities of $\mathbf{c}$ and $\mathbf{c}_g$, respectively, as shown. The rotated axes (x', z') are used to derive amplitude solutions for the small wave as it propagates through the big wave.

$$A(c_{gz} - C_z) = \text{const}, \tag{21}$$

where $c_{gz} = c_{gz}^{+}$. This solution determines the amplitude of the small-scale gravity wave along its path through the tide in the absence of saturation. These solutions provide a convenient initial check of our numerical ray method of evaluating A within more general environments, as described in Appendix A.

Note that (21) is singular whenever $c_{gz} = C_z$ (i.e., $A \rightarrow \infty$). This "phase-group condition" produces ray caustics and has been interpreted in oceanic studies as a reflection point in the (x'', z'') frame which produces "separatrix crossings" and permanent changes in m and ω^{+} [*Broutman and Young*, 1986; *Broutman*, 1986; *Broutman and Grimshaw*, 1988; *Bruhwiler and Kaper*, 1995]. Phase-group caustics do not occur here because both the tide and the gravity wave always propagate their energy upward, so c_{gz} and C_z are antisigned and never equal.

Results for Constant Tidal Amplitudes

Diurnal Tide

We consider first a diurnal tide ($n = 1$) of peak amplitude $\hat{U}_{\text{TIDE}} = 20$ m s^{-1} and $\Lambda_z = 2\pi/M = 40$ km. These tidal parameters are fairly typical of the midlatitude winter mesosphere [e.g., *Vincent et al.*, 1988; *Manson et al.*, 1989], so we choose $y = 45°$N initially. Figure 2a plots contours of the height-time zonal velocity oscillation of the tide.

The remaining curves throughout Figure 2 show the height variations of a range of gravity-wave-related variables which

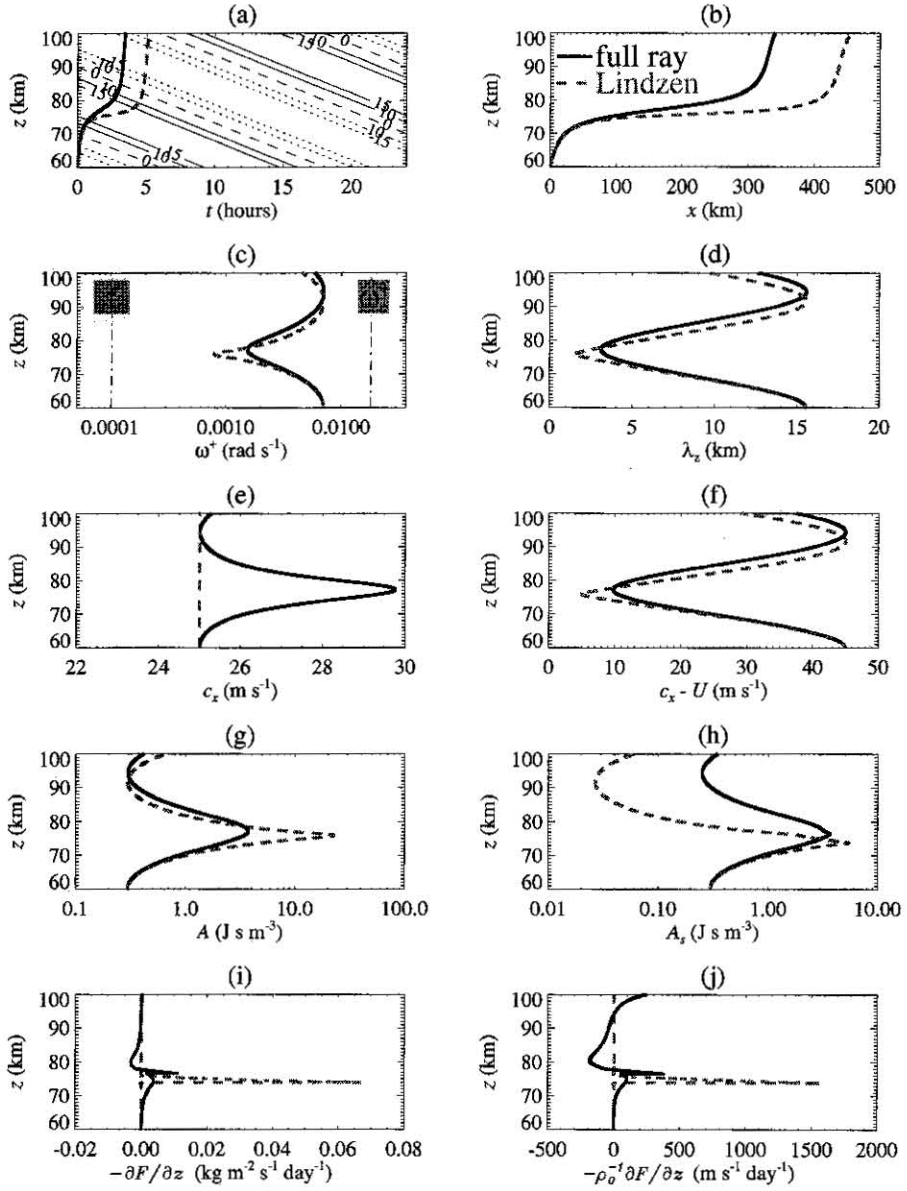

Figure 2. Variations with height along the ray path of various wave parameters of a gravity wave propagating through tidal zonal velocities (contour labels in Figure 2a are in meters per second and solid (dotted) contours depict positive (negative) tidal winds). The results of two ray solutions are depicted: the Lindzen solution (dashed curve) and the full ray solution (solid curve). At $z = 60$ km, $\overline{u'^2} + \overline{v'^2} = 7$ m^2 s^{-2} for both solutions. (a) Tidal velocities are contoured; curves depict ray loci through these diurnal tidal winds, (b) spatial trajectory, (c) intrinsic frequency, (d) vertical wavelength, (e) ground-based zonal phase speed, (f) intrinsic zonal phase speed, (g) unsaturated action density, (h) saturation-scaled action density, (i) Eliassen-Palm flux divergence, and (j) mean-flow acceleration.

resulted from tracing a gravity wave through these tidal winds. The solid curves show the full ray solution, while the dashed curves show the Lindzen solution for the same wave. In each instance we launched the wave zonally ($l = 0$) at $z = 60$ km and $t = 0$ with an initial horizontal wavenumber $k = 2\pi$ (40 km)$^{-1}$, an initial ground-based horizontal phase speed $c_x = \omega/k$ of 25 m s^{-1}, and an initial horizontal-velocity variance $\overline{u'^2} + \overline{v'^2} = 7$ m^2 s^{-2}. The wave is launched at a trough of the tidal velocity oscillation, at which $\partial m/\partial z = 0$ initially (see Appendix A).

The resulting time-height ray loci are superimposed upon the tidal velocity contours in Figure 2a, while the spatial trajectories of each solution are shown in Figure 2b. Note that the group trajectories of the two solutions differ considerably. These differences reflect the important effects of tidally induced background accelerations $\partial U'_{\mathrm{TIDE}}/\partial t$ on the ray path of the gravity wave. In other words, the Lindzen solutions give inaccurate ray paths through the tide.

The remaining panels in Figure 2 show the variation with height along the ray path of various gravity wave parameters. We note that the refractive excursions in ω^+ and $\lambda_z = 2\pi/m$ (Figures 2c and 2d, respectively) are smaller for the full ray solution than for the Lindzen solution. The reason for this is illustrated by the $c_x = \omega/k$ variations in Figure 2e. While the ground-based zonal phase speed c_x is invariant for the *Lindzen* [1981] solution, it varies in the full ray solution since k is nearly

constant, but ω varies according to (2), or equivalently in this case, according to the solution (19). A region of positive tidal shear ($U_z > 0$), which refracts waves to a larger wavenumber $|m|$ through (1) (since $m < 0$), is also a region of positive tidal acceleration ($U_t > 0$), which refracts waves to higher frequencies and larger c_x values through (2). The two effects have opposing influences on ω^+ and combine to reduce the range of refraction of ω^+ and λ_z compared to the time-invariant Lindzen solution. However, one should note that if tidal phase moved upward, then $U_t < 0$ when $U_z > 0$, whereupon the full ray solution undergoes greater variations in ω^+ and λ_z than the Lindzen solution.

As an extreme example of the importance of tidal accelerations on gravity wave paths, consider allowing $\Lambda_z \to \infty$, so that $dm/dt \to 0$ according to (1). Thus m remains constant and, since κ_h is also nearly constant, then the intrinsic frequency ω^+ remains constant through the dispersion relation (20), despite the presence of time-varying background winds. This constancy is achieved through refraction of ω values through (2), which in this case has the solution $\omega(t) = \omega(t_0) + k[U(t) - U(t_0)]$. Since $\omega^+ = \omega - kU$, then ω^+ remains constant [e.g., *Jones*, 1969; *Zhong et al.*, 1995].

The reduced variations in ω^+ due to the temporal oscillation of the tide (Figure 2c) also influence the stability and saturation of the gravity wave, since in these simulations the wave saturates when

$$\overline{u'^2} + \overline{v'^2} \geq \tfrac{1}{2}|c_x - U|^2 = \frac{\omega^{+2}}{2k^2}, \tag{22}$$

(assuming $l^2 \ll k^2$). Since k remains constant, the saturation threshold in (22) varies according to the ω^+ variations. Figure 2f plots the variations in the intrinsic horizontal phase speed $|c_x - U| = |\omega^+/k|$. We see again that waves governed by the Lindzen solution are refracted to smaller intrinsic phase speeds, so they will be rendered unstable at much smaller wave amplitudes than the full ray solutions, according to (22). Consequently, dissipation is more likely in the Lindzen solutions.

Figure 2g shows the gravity wave action density A, evaluated in the absence of any dissipative processes. We note that the enhancements of A in the full ray solution, at tidal phases where c_{gz} slows due to refraction, are much smaller than in the Lindzen solution. This effect also makes the waves governed by a Lindzen solution much more susceptible to saturation, since their action densities and associated velocity variances become much larger in response to refraction than those governed by the full ray solution. The combined results in Figures 2f and 2g indicate that waves governed by a Lindzen solution are rendered unstable more readily and more suddenly by tidal refraction than similar waves governed by the full ray solutions. Clearly, the time variations of the tidal oscillation have a stabilizing influence on the GW-tidal interaction, so Lindzen solutions overestimate tidally modulated gravity wave breaking.

Figure 2h shows the results of applying saturation limits to the action densities of each ray solution. As expected, the Lindzen solution is more suddenly and dramatically dissipated at ~74 km. To quantify the resultant mean-flow accelerations, we first evaluate the vertical flux of zonal pseudomomentum density,

$$F = kc_{gz}A. \tag{23}$$

It can be shown that $-F$ in (23) equals the vertical component of the EP flux, the divergence of which determines the acceleration of the zonally averaged background flow [e.g., *Andrews and McIntyre*, 1976]. Since here the EP flux divergence simplifies to $-\partial F/\partial z$, we have approximated it in Figure 2i by differencing successive F values along the ray path. An exact calculation of $-\partial F/\partial z$ again requires a ray tube calculation; we shall show later that this approximate along-ray calculation is reasonably accurate in this case.

The Lindzen solution exhibits a strong and narrow layer of EP flux divergence and mean-flow acceleration ($-\rho_0^{-1}(z)\partial F/\partial z$, shown in Figure 2j) at ~74 km and no response elsewhere. Conversely, the full ray solution shows a smaller impulsive mean-flow acceleration due to saturation at ~77 km. However, this is superimposed upon a smoothly varying oscillatory mean-flow acceleration, which arises in spite of an absence of any dissipation of A away from the narrow layer at ~77 km. This latter feature arises due to the transience in the problem and is addressed in the following section.

Transient EP Flux Effects

The EP flux divergences that arise in the full ray solution away from regions of wave saturation in Figure 2i can be explained by first multiplying the wave-action equation (8) by k. Since horizontal gradients are zero here and k is invariant with height, this yields

$$\frac{\partial}{\partial t}(kA) = -\frac{\partial F}{\partial z}, \tag{24}$$

in the absence of wave dissipation ($\tau^{-1} = 0$). Equation (24) has the same form as the generalized EP theorems sought in various three-dimensional studies of wave phenomena [e.g., *Haynes*, 1988; *Scinocca and Shepherd*, 1992]. Nonacceleration conditions require $\partial F/\partial z = 0$, but (24) shows that the transience in the wave pseudomomentum density induced by the tidal oscillation [$\partial(kA)/\partial t \neq 0$] yields $\partial F/\partial z \neq 0$ and a mean-flow forcing.

This mean-flow forcing due to transient pseudomomentum densities differs from previous studies of these effects [e.g., *Jones and Houghton*, 1971; *Andrews*, 1980; *Coy and Hitchman*, 1984; *Dunkerton and Fritts*, 1984] in that the transience is not preimposed but is periodically induced by tidal refraction. This leads to gravity wave EP flux divergences which are highly phase coherent with the tidal oscillation (as illustrated later; see Figure 3a), which raises some important questions concerning their possible effects on tidal wind profiles. We investigate this further here, keeping in mind the likely limitations of our noninteractive small-amplitude slowly varying ray model in fully specifying transient wave mean-flow interactions [*Fritts and Dunkerton*, 1984; *Fritts et al.*, 1996].

We first express the total zonal momentum balance of the larger-scale flow as

$$\frac{\partial(\bar{U} + \mathcal{U}'_{\mathrm{TIDE}})}{\partial t} - f\bar{V} + \frac{1}{\rho_0}\frac{\partial \mathcal{P}'_{\mathrm{TIDE}}}{\partial x} = -\frac{1}{\rho_0}\left(\bar{D} + \frac{\partial F}{\partial z}\right). \tag{25}$$

Here $(\bar{U}, \bar{V})$ is the zonally averaged wind profile, and $\bar{D}$ is the mean zonal body force which sustains the mean winds. We assume for simplicity that $\bar{D}$ results from saturation of small-scale gravity waves and does not influence the tidal profile. The extra EP flux divergence term in (25) results from tidally induced transience of a nondissipating gravity wave. We assume that the same wave is launched with the same amplitude at equispaced longitudes around a latitude circle. In this case, $\partial F/\partial z$ averages to 0 over one horizontal oscillation of the tide

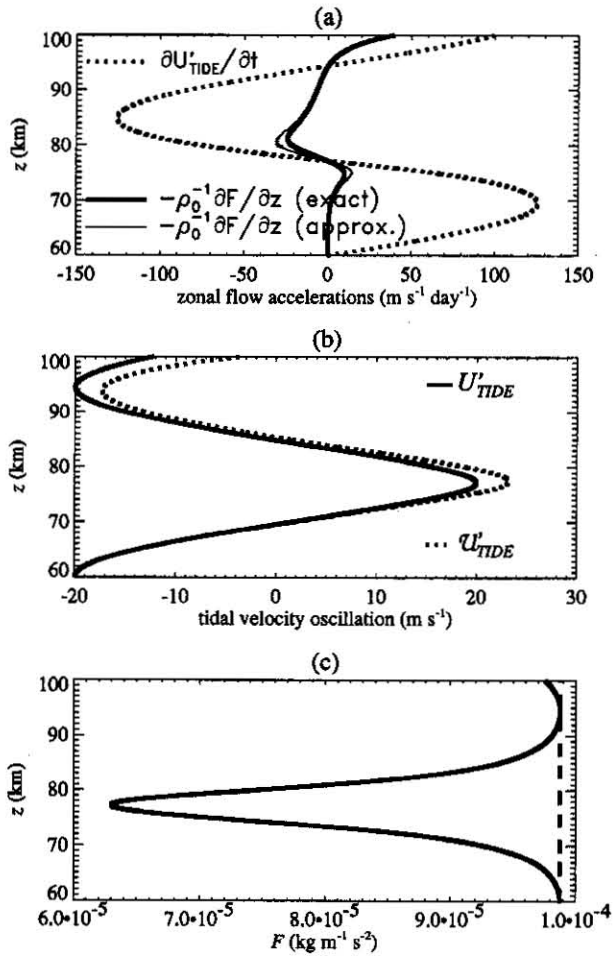

Figure 3. Variations with height of various GW and tidal parameters, as encountered along the gravity wave path in Figures 2a and 2b: (a) zonal accelerations due to the tide ($\partial U'_{\mathrm{TIDE}}/\partial t$, dotted curve) and transient GW-induced flow accelerations $-\rho_0^{-1}\partial F/\partial z$ (exact solution (27), thick solid curve, and the along-ray approximation, thin curve); (b) tidal winds along the ray path; original tidal velocity U'_{TIDE} (solid curve) and modified velocity wave $\mathcal{U}'_{\mathrm{TIDE}}$ (dotted curve); and (c) upward flux of zonal pseudomomentum density F for the full ray solution (solid curve) and for the Lindzen solution (dashed curve). At $z = 60$ km, $\overline{u'^2} + \overline{v'^2} = 1$ m^2 s^{-2}.

and does not contribute to $\bar{D}$. For generality, we have assumed a tidal velocity wave $\mathcal{U}'_{\mathrm{TIDE}}$ and pressure wave $\mathcal{P}'_{\mathrm{TIDE}}$ which can differ from the original values U'_{TIDE} and P'_{TIDE} as a result of this transient EP flux term. Note too that we assume $K \neq 0$ in (25) and we have omitted the advective term $\bar{U}\partial/\partial x(\mathcal{U}'_{\mathrm{TIDE}})$ since it is usually small.

Strictly, (25) only holds for zonally averaged flows: A full three-dimensional wave mean-flow interaction theory does not currently exist [*Scinocca and Shepherd*, 1992]. However, the applicability of (25) in three dimensions is fundamental to nearly all current specifications of GW-drag effects on three-dimensional atmospheric circulations [see, e.g., *Holton*, 1984; *Smith*, 1996].

Factoring out the zonally averaged terms in (25) yields the tidal momentum balance equation

$$\frac{\partial \mathcal{U}'_{\mathrm{TIDE}}}{\partial t} + \frac{1}{\rho_0}\frac{\partial \mathcal{P}'_{\mathrm{TIDE}}}{\partial x} = -\frac{1}{\rho_0}\frac{\partial F}{\partial z}, \tag{26}$$

where for simplicity, we have neglected any meridional velocity response of the tide to the transient gravity wave forcing. It should be noted that strictly, another dissipation term should be included on the right of (26) to account for the constant amplitude with height of the original tidal oscillation (rather than an exponential increase $\propto \rho_0^{-1/2}(z)$ that would occur in the absence of some preexisting tidal dissipation).

Thus (26) implies that these transient gravity wave EP flux divergences affect the tide and not the mean flow, consistent with previous nontransient saturation studies of GW-tidal interactions [e.g., *Fritts and Vincent*, 1987]. These EP flux divergences, approximated in Figure 2i by along-ray differencing, can be evaluated exactly in the case of constant tidal amplitude and no gravity wave saturation by manipulating (24), based on our analytical action solution (21), to give

$$\begin{aligned} -\frac{\partial F}{\partial z} &= k\frac{\partial A}{\partial t}, \\ &= -kC_z\frac{\partial A}{\partial z}, \\ &= \left(\frac{kC_zA}{c_{gz}-C_z}\right)\frac{\partial c_{gz}}{\partial z}, \end{aligned} \tag{27}$$

which can be evaluated exactly with the aid of our ray-tracing method for computing $\partial c_{gz}/\partial z$, as described in Appendix A.

To study this, an identical ray trace to that in Figure 2 was performed, except that in this case the gravity wave had an initial variance $\overline{u'^2} + \overline{v'^2} = 1$ m^2 s^{-2} at 60 km. This smaller initial variance results in no saturation of the full ray solution between 60 and 100 km, so that the EP flux divergences of this gravity wave solution are due entirely to the transience induced by tidal accelerations. Figure 3a shows the zonal accelerations of the original tidal oscillation, $\partial U'_{\mathrm{TIDE}}/\partial t$ (dotted curve), as computed along the ray trajectory. Zonal accelerations due to transient gravity wave EP flux divergences induced by this tidal oscillation are also plotted, using both the exact solution (27) (solid curve) and an approximation obtained by along-ray differencing (thin curve). Note that the differencing calculation slightly overestimates $-\rho_0^{-1}\partial F/\partial z$.

We see that $\partial U'_{\mathrm{TIDE}}/\partial t$ and $-\rho_0^{-1}\partial F/\partial z = \rho_0^{-1}\partial(kA)/\partial t$ have a similar vertical wavelength and are essentially in phase, although $-\rho_0^{-1}\partial F/\partial z$ is clearly nonsinusoidal and peaks at different heights. This in-phase relationship tends to enhance the total diurnal accelerations of the flow. To quantify this, we first rearrange (26) with the aid of (24) to give us

$$\frac{\partial}{\partial t}\left(\mathcal{U}'_{\mathrm{TIDE}} - \frac{kA}{\rho_0}\right) + \frac{1}{\rho_0}\frac{\partial \mathcal{P}'_{\mathrm{TIDE}}}{\partial x} = 0. \tag{28}$$

On invoking (28) at times t_1 and t_2, during which we assume that $\partial \mathcal{P}'_{\mathrm{TIDE}}/\partial x$ is constant, then it follows that

$$\begin{aligned} \mathcal{U}'_{\mathrm{TIDE}}(x, z, t_2) \approx{}& \mathcal{U}'_{\mathrm{TIDE}}(x, z, t_1) \\ &+ \frac{k[A(x, z, t_2) - A(x, z, t_1)]}{\rho_0(z)}. \end{aligned} \tag{29}$$

We now assume that $U'_{\mathrm{TIDE}}(x, z, t)$ returns after this unsaturated wave activity has propagated through the tide ($A \rightarrow 0$) [e.g., *Andrews*, 1980], even though no smooth transition to $A = 0$ occurs in the present problem. This yields [e.g., *Andrews*, 1980; *Dunkerton*, 1981; *Dunkerton and Fritts*, 1984]

$$\mathcal{U}'_{\mathrm{TIDE}}(x, z, t) \approx U'_{\mathrm{TIDE}}(x, z, t) + \frac{kA(x, z, t)}{\rho_0(z)}, \tag{30}$$

and $\partial \mathcal{P}'_{\mathrm{TIDE}}/\partial x = \partial P'_{\mathrm{TIDE}}/\partial x$. Thus we see that time-varying gravity wave pseudomomentum densities due to refraction by the tidal wind profile produce accompanying accelerations or decelerations of the tidal wind profile which are temporary and reversible.

Figure 3b shows U'_{TIDE} as a function of height, as encountered along the ray trajectory in Figure 2a. The dotted curve shows $\mathcal{U}'_{\mathrm{TIDE}}$, evaluated from (30), illustrating that the transient $\rho_0^{-1}\partial(kA)/\partial t$ term is large at the tidal peak and tends to enhance it. The similar mean-flow acceleration at the tidal trough at ~95 km in Figure 3b is due to the amplification of a smaller pseudomomentum density kA by the smaller background densities $\rho_0(z)$ at these heights, according to (30).

To show these effects more clearly, Figure 4 plots time variations of the action density A, tidal velocities U'_{TIDE} and $\mathcal{U}'_{\mathrm{TIDE}}$, and pseudomomentum flux F at a fixed height of 80 km. Evaluating time variations at a given height requires that we launch a number of rays at successive time intervals. However, the results in Figure 4 were produced by extrapolating the results of a single ray integration by noting that for a constant tidal amplitude, ray paths at later launch times follow by translating the ray loci of the earlier solution in Figure 2a along the phase motion of the tide to later times. Figure 4b again shows, more clearly this time, that the tidal peaks are enhanced by the transient gravity wave forcing.

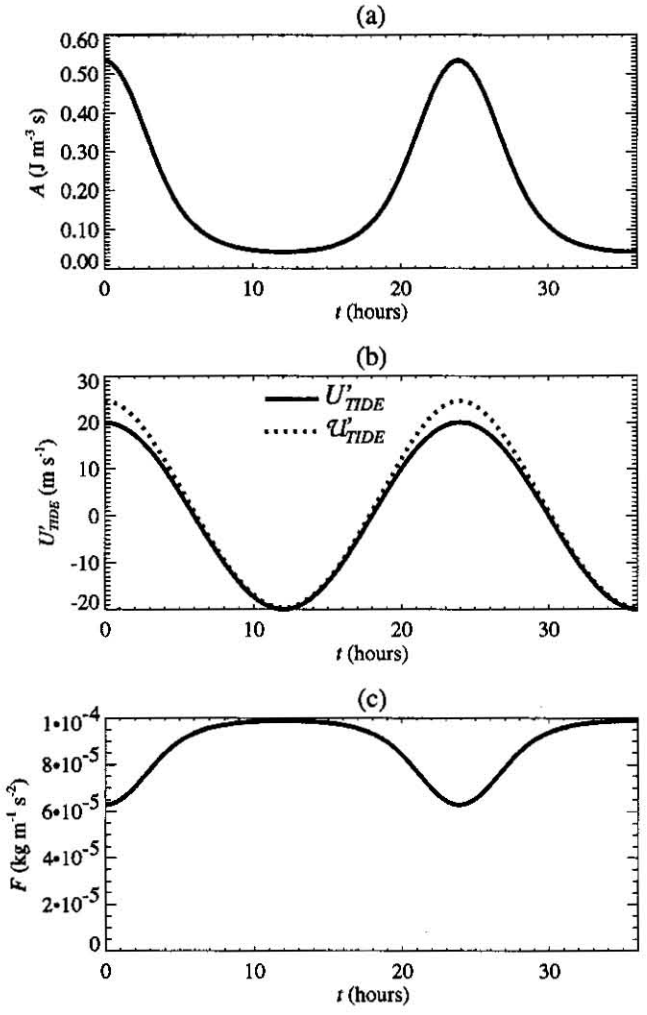

Figure 4. Time variations of GW and tidal parameters at z = 80 km for a continuous train of gravity waves: (a) action densities A; (b) tidal velocity wave U'_{TIDE} (solid curve) and modified velocity wave $\mathcal{U}'_{\mathrm{TIDE}}$ (dotted curve); and (c) zonal GW pseudomomentum flux densities F.

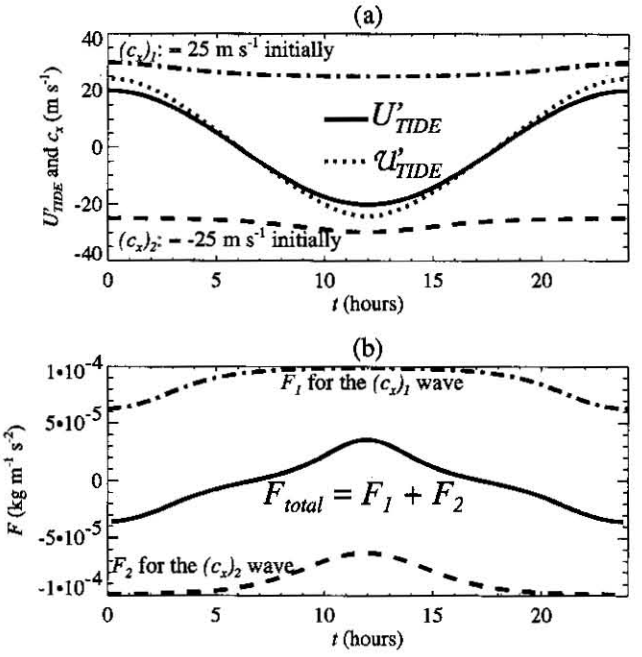

Figure 5. Simulation similar to that in Figure 4 but using two oppositely propagating gravity waves with phase speeds $(c_x)_1$ and $(c_x)_2$. (a) Time variations of (c_x), (dashed-dotted curve) and $(c_x)_2$ (dashed curve) are plotted at z = 80 km. Tidal velocity wave U'_{TIDE} (solid curve) and modified velocity wave $\mathcal{U}'_{\mathrm{TIDE}}$ (dotted curve) are also shown. (b) Time variations of F for each wave (F_1 and F_2) and their sum F_{total}.

Note that if we were to launch this same gravity wave with an oppositely directed phase speed ($c_x = -25$ m s^{-1} initially), its tidally induced transience will enhance the troughs of the tidal velocity wave. Clearly, then, both waves acting in concert tend to enhance both the peaks and the troughs of the tide and thus amplify the local tidal wind oscillation. The results of such a two-wave simulation are shown in Figure 5: Figure 5a shows U'_{TIDE} and $\mathcal{U}'_{\mathrm{TIDE}}$ at 80 km, the latter resulting from the combined transience of two gravity waves with initial c_x values of $(c_x)_1 = 25$ m s^{-1} (the original ray solution) and $(c_x)_2 = -25$ m s^{-1}. The $(c_x)_2$ wave was launched at 40 km with an appropriately scaled-down initial amplitude, so that both waves had the same initial intrinsic phase speed and equal and opposite diurnally averaged EP fluxes at each height. The time variations of $(c_x)_1$ and $(c_x)_2$ due to tidal accelerations are also plotted in Figure 5a. Note particularly the overall enhancement of the local tidal wind oscillation due to the combined transient variations of both gravity wave EP fluxes. However, note again that these enhancements are temporary; whether permanent changes in tidal amplitudes are possible is discussed later.

We conclude here by considering whether there is any observational support for the transient gravity wave dynamics we have described here. Figures 3c, 4c, and 5b plot the pseudomomentum flux densities F. On comparing these curves with the tidal velocity waves in Figure 3b, 4b, and 5a, respectively, we note clear anticorrelations between F and the tidal velocity

U'_{TIDE}. Since there was no saturation in these particular ray integrations, these anticorrelations arise solely from the transience in the gravity wave amplitudes induced by the tidal accelerations (for example, $F_{\mathrm{total}} = F_1 + F_2$ in Figure 5b is uniformly zero using nondissipating Lindzen solutions). This anticorrelation is a robust result; it occurs in varying degrees within all of our simulations. Note particularly from Figure 5b that the anticorrelations occur regardless of the direction of horizontal phase propagation of the gravity wave.

The gravity wave EP flux $-F = -\rho_0 \overline{u'w'}$ for $f^2 \ll \omega^{+2} \ll N^2$, where u' and w' are zonal and vertical velocity perturbations, respectively, of the gravity wave motion [e.g., *Fritts and Vincent*, 1987]. Since the covariance $\overline{u'w'}$ can be measured, this permits observations of F within tidal velocity fields. Mesospheric radar measurements have revealed that anticorrelations between F and U'_{TIDE} are a characteristic feature of the data [see, e.g., *Wang and Fritts*, 1991]. To date, such observations have been explained in terms of tidally modulated gravity wave saturation [e.g., *Fritts and Vincent*, 1987; *Lu and Fritts*, 1993; *Fritts*, 1995]. Our results suggest that some of this observed variability may also be due to gravity wave transience which is induced by the time-varying refraction of gravity waves by tidal wind oscillations. We note again that the mechanism we have described here will operate regardless of whether the wave field is dissipating or stable and regardless of the horizontal propagation directions of the waves.

Numerical Results for Height-Varying Tidal Amplitudes

We now study the interaction of a gravity wave with a more complicated tidal structure. We adopt a Gaussian vertical profile of tidal amplitude in (7) of the form

$$U_{\mathrm{TIDE}}(z) = U_{\max} \exp\left(\frac{-(z - z_{\max})}{L}\right)^2. \qquad (31)$$

This time we consider a semidiurnal tide ($n = 2$) of $\Lambda_z = 2\pi/M = 100$ km and amplitude governed by (31), with $U_{\max} = 20$ m s^{-1}, $z_{\max} = 80$ km, and $L = 30$ km. This yields tidal variations in reasonable agreement with mesospheric data during summer at 35°S [e.g., *Vincent et al.*, 1988], although one should note that significant semidiurnal tidal activity often persists well into the thermosphere [e.g., *McLandress et al.*, 1996]. These tidal winds are contoured in Figure 6a.

The transformation sequence $(x, z) \rightarrow (x'', z'')$ now no longer eliminates time variations in the (x'', z'') frame, since the amplitude profile (31) moves upward with time when viewed from this frame. Consequently, we must now resort solely to numerical ray integrations to obtain gravity wave solutions.

We start the rays in these simulations from an artificial lower height of $z = -50$ km, where $U(z, t)$ and its height-time gradients are all extremely small. We launch rays of identical characteristics, so that rays emanating from well below the tide are initially monochromatic and plane-parallel ($\partial m/\partial z = 0$). In this way the ray integrations from $z = -50$ km to the surface are a numerical technique for establishing accurate initial conditions for the wave at the ground under these assumptions.

Figure 6 shows the results of a numerical ray integration, with variations of parameters along the ray plotted in the height range 0–100 km. The wave had identical original parameters to the one traced in Figure 2, except that it was launched at $t = 0$ and $z = -50$ km with an initial $\overline{u'^2} + \overline{v'^2}$ that grows to 7 m^2 s^{-2} at $z = 60$ km in the absence of any refraction. This choice ensures that the wave-action densities here are of similar magnitude to those in Figure 2.

Below ~40 km, where $U(z, t)$ is small, we note that the Lindzen and full ray solutions agree. Above this height, where the time-varying tidal amplitudes become significant, we note again that the two solutions diverge significantly from each other.

To study the behavior of the full ray solutions in greater depth, Figure 7a shows time-height ray loci for a sequence of successive ray integrations for this wave that commenced at $z = -50$ km at regular 15-min intervals. Again, the tidal velocity oscillation through which the waves propagate is contoured on the plot. This time the waves are traced to a height of 150 km, where the tidal oscillation is almost completely absent. This is done purely to provide a "far field" from the tide which allows us to gauge whether interaction with the tide permanently affects the emergent wave activity. Consequently, no attempt has been made to include ionospheric processes into the background atmosphere at heights ≥100 km.

The ray loci in Figures 7a and 7b reveal that permanent changes in the ray paths result from the interaction with the tide, so that at ~150 km there is a periodic (semidiurnal) focusing and defocusing of ray paths that were all initially parallel. While the ray focusing events in Figure 7a look like possible caustics, they are not, as evident in Figure 7b, while Figure 7f shows that WKB requirements are satisfied. The focusing of rays implies a compression of wave packets and a consequent buildup of wave amplitude, whereas reduced amplitudes should occur during the defocusing phase as packet widths broaden. The action solutions in Figure 7c bear this out. Note again that these time-varying action densities result solely from time-varying tidal accelerations acting on the ray paths. The horizontal line in Figure 7c shows the time-mean action density of all the rays at ~150 km, which also equals the uniform A values that occur here when Lindzen solutions are used to evaluate the ray paths. Figure 7e shows a similar collection of curves for ω^+.

The time-varying ray characteristics at 150 km occur because the packet width of the tide is of the order of the vertical tidal wavelength ($L/\Lambda_z \sim 1$). When $L/\Lambda_z \gg 1$, the time variations of the emergent wave activity are substantially reduced because, after propagating through many tidal cycles during which tidal amplitudes change only slowly, the time-varying refraction terms tend to average out to a near-zero net effect on the gravity wave.

The time-varying A values at 150 km imply transient mean-flow forcing of a form proportional to $\partial A/\partial t$, which is shown in Figure 7d. The buildup of action densities during focusing phases also suggests that fairly intense wave breaking will occur at times of ray focusing. Since the focusing is periodic, such wave breaking may force a wave motion, particularly in the presence of a second oppositely propagating gravity wave as in Figure 5. On inspecting the upward sloping time-height focusing regimes in Figure 7a, wave breaking within these regions would tend to produce a semidiurnal wave with upward phase propagation and a very long vertical wavelength. If this produced an internal gravity wave mode, this wave would propagate to lower heights. However, since the forcing is also highly nonsinusoidal (Figure 7d), the response to this forcing may be more complicated.

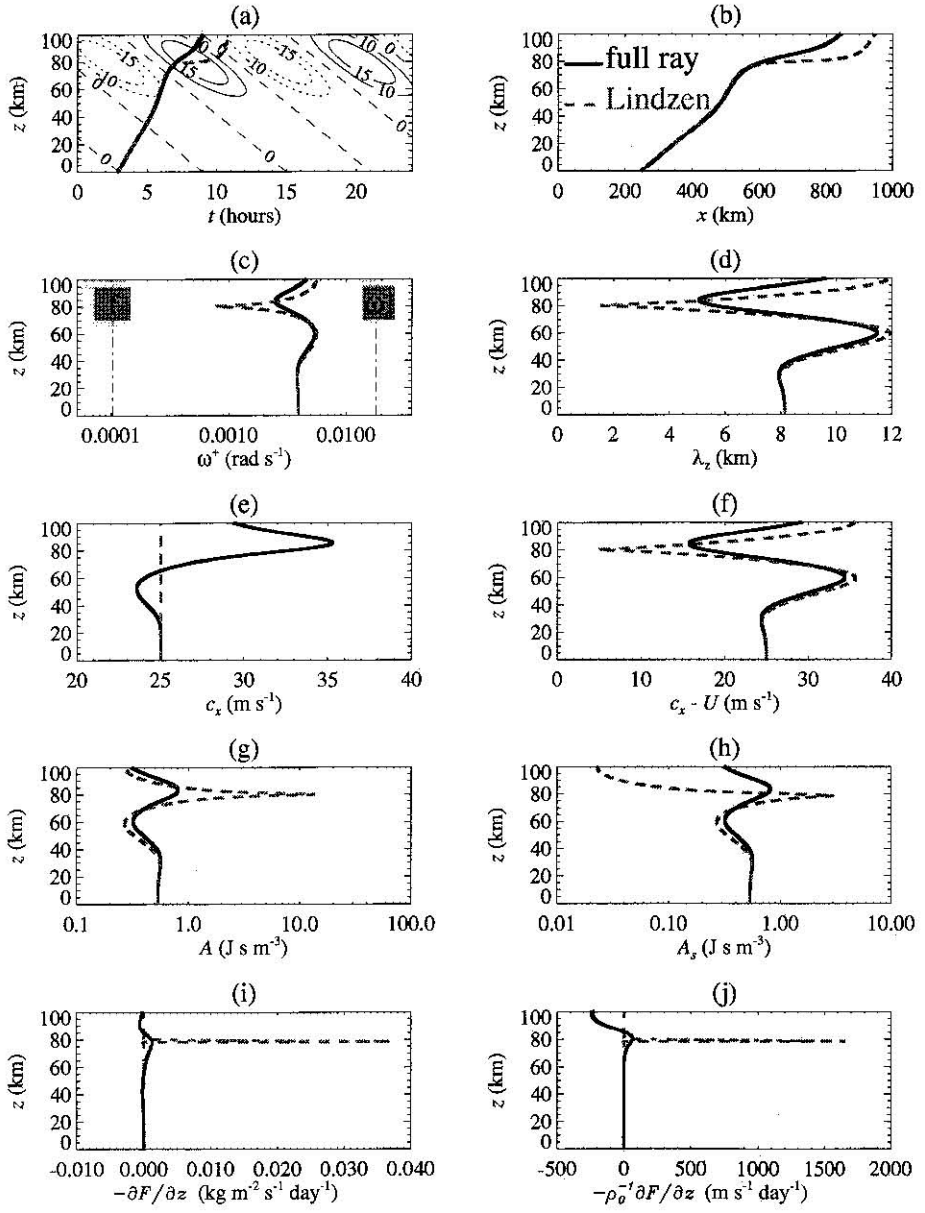

Figure 6. As for Figure 2, but for a semidiurnal tide with $\Lambda_z = 2\pi/M = 100$ km and a Gaussian amplitude profile governed by (31), with $U_{max} = 20$ m s^{-1}, $z_{max} = 80$ km, and $L = 30$ km. Results are plotted from the ground to $z = 100$ km. (a) Ray loci through semidiurnal tidal winds, (b) spatial trajectory, (c) intrinsic frequency, (d) vertical wavelength, (e) ground-based zonal phase speed, (f) intrinsic zonal phase speed, (g) unsaturated action density, (h) saturation-scaled action density, (i) Eliassen-Palm flux divergence, and (j) mean-flow acceleration.

Discussion

Lindzen Parameterizations of GW-Tidal Interactions

The ray simulations have illustrated that Lindzen solutions often differ markedly from the full ray solutions within a time-varying tidal background. This raises some doubts about the accuracy of the *Lindzen* [1981] parameterization (and subsequent variants of it) in modeling GW-tidal interactions.

The Lindzen parameterization remains popular among modelers because of its simplicity and its generally good performance in simulating mean circulation profiles within arbitrary environments. This contrasts with the simulations conducted here, which needed a fairly complicated numerical model to accurately solve a highly idealized problem. Thus we consider here whether current implementations of the Lindzen parameterization can be modified, rather than overhauled or replaced, to include some of the time-varying effects we have reported here, while retaining some of the attractive simplicity of the current parameterization.

Of the many changes to gravity wave solutions that arise on including background time variations there are two major ones which have important consequences for the *Lindzen* [1981] parameterization. The first is the different solution of the wave-action equation (8). The Lindzen GW-drag formulae are derived from the solution (12) [e.g., *Schoeberl*, 1985], which follows from (8) on neglecting x, y, and t variations in the background atmosphere. Retention of time-varying terms re-

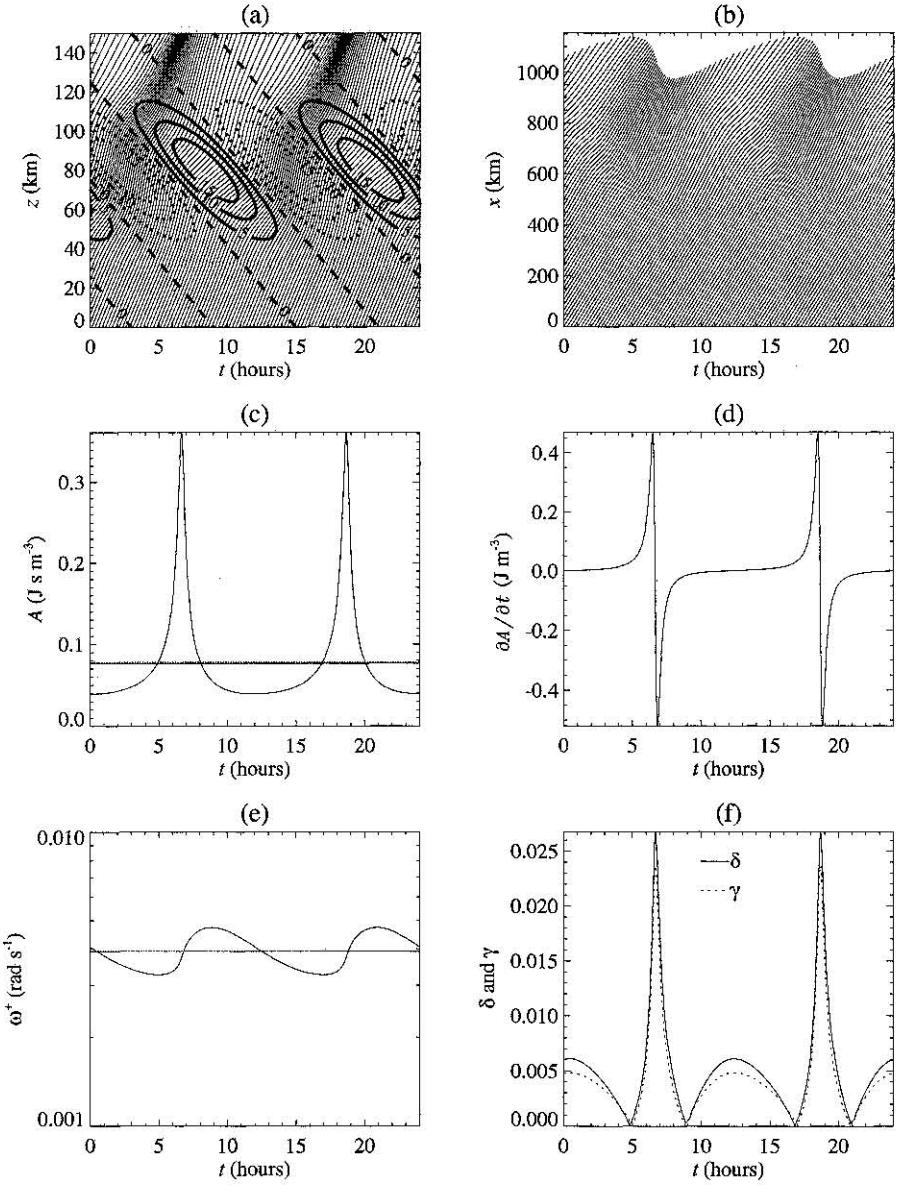

Figure 7. Multiray simulation through the same tidal profile as in Figure 6. (a) Zonal tidal winds are contoured from the ground to 150 km; thin curves show various ray loci through these semidiurnal tidal winds, (b) horizontal trajectories; $x - t$ loci of the various rays traced through the tide, (c) action densities, A, (d) rate of change of A, $\partial A/\partial t$, (e) intrinsic frequencies, ω^+, and (f) WKB parameters δ and γ. Figures 7c–7f show time variations of the ray parameters at $z = 150$ km.

quires a numerical solution of (9), as described in Appendix A. Although analytical solutions to (9) can be derived for certain problems, such as (16) in the case of a constant tidal amplitude, even these solutions have possible ramifications for the gravity wave driving of the larger-scale flow which are difficult to delineate fully at present. As any general implementation of (9) would require a major overhaul of the Lindzen parameterization, we investigate here whether improvements can result without changing the current GW-drag formulae based on (12).

A second major effect of time variations is that ground-based horizontal phase speeds c_x vary in response to background accelerations, as shown in Figures 2e and 6e [see also *Jones and Houghton*, 1971; *Fritts and Dunkerton*, 1984; *Walterscheid and Schubert*, 1990; *Zhong et al.*, 1995]. By contrast, the Lindzen theory assumes no background time variations, so c_x is taken to be constant with height. Variations in c_x are important because the parameterization formulae of *Lindzen* [1981] are especially sensitive to phase speed values; for example, the turbulent diffusivities that result from wave breaking scale as $|c_x - U|^4$.

Representative variations in c_x can be incorporated fairly easily into the Lindzen parameterization. One simple possible implementation is described and discussed in Appendix B. To see whether including transient c_x variations alone leads to a better comparison with a full ray solution, Figure 8 reproduces the simulation of Figure 2 but includes an extra solution (the thick dotted curve) in which the full trajectory solution is used (i.e., c_x can vary), but wave amplitudes are governed by the time-invariant solution (12). Clearly, the inclusion of variable c_x values improves the simulation. Thus an adapted Lindzen

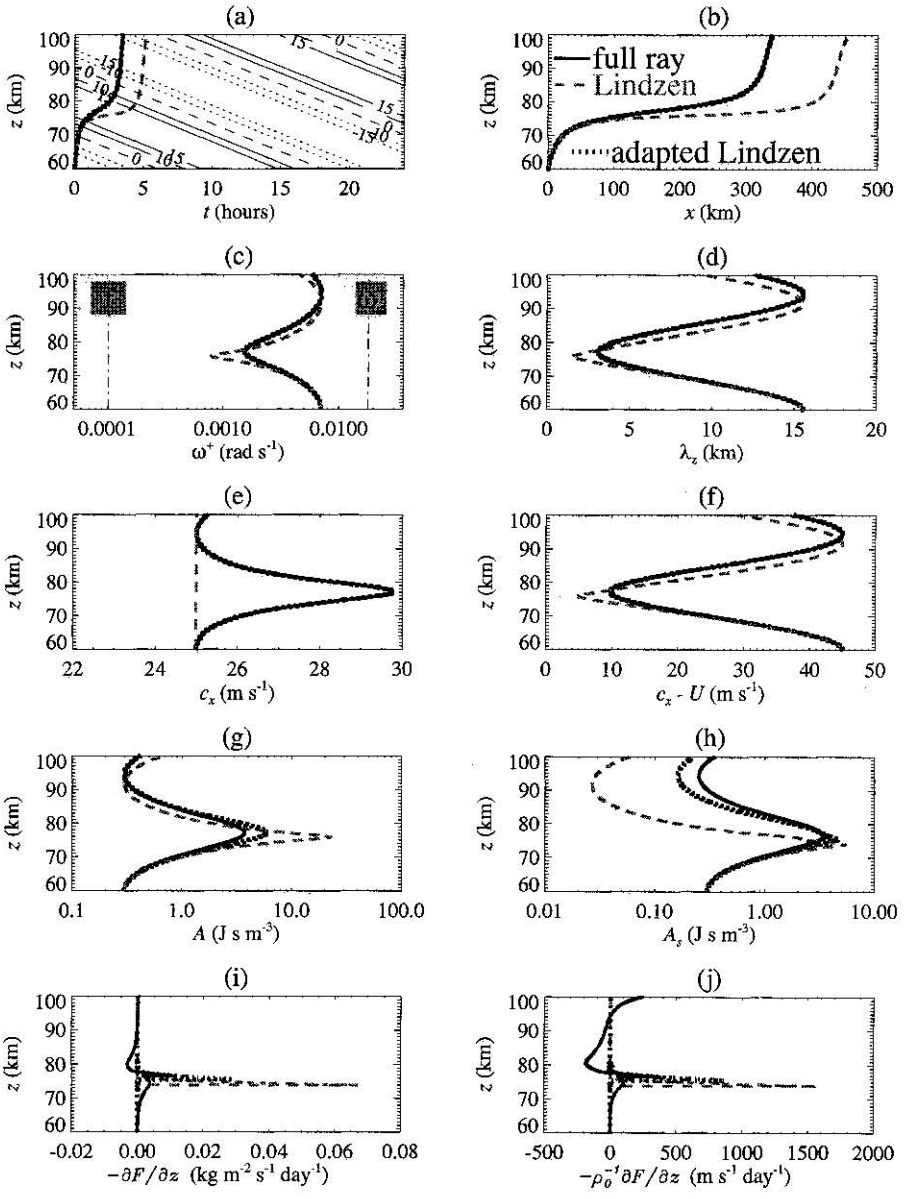

Figure 8. As for Figure 2, but including a third solution in which the full ray solution is used for the ray path (so that c_x variations are included). However, the Lindzen-like solution (12) is used to govern the wave amplitude. This "adapted Lindzen" solution is plotted with a thick dotted curve, in addition to the original full ray solution (solid curve) and Lindzen solution (dashed curve). (a) Ray loci through diurnal tidal winds, (b) spatial trajectory, (c) intrinsic frequency, (d) vertical wavelength, (e) ground-based zonal phase speed, (f) intrinsic zonal phase speed, (g) unsaturated action density, (h) saturation-scaled action density, (i) Eliassen-Palm flux divergence, and (j) mean-flow acceleration.

parameterization, in which the original amplitude formulae are retained but c_x values may vary, should result in more accurate simulations of gravity-wave interactions with tides.

Transient GW-Induced Tidal Accelerations

The ray-tracing experiments simulated time-varying EP flux divergences for a gravity wave as it propagated through a tide. It was shown that this produced zonal accelerations which were highly phase coherent with the tide, and it was argued that they temporarily amplified the tide.

For permanent tidal amplification or attenuation to occur the total energy density of the gravity wave packet must be changed by the interaction. If A behaves conservatively ($\tau^{-1} = 0$), then this requires a net change in ω^+ [e.g., *Broutman and Young*, 1986]. *Broutman and Young* [1986] and *Broutman and Grimshaw* [1988] found large permanent increases in ω^+ for oceanic gravity waves propagating through an inertial oscillation, but these required $c_{gz} = C_z$ somewhere along the ray path, which cannot occur in these simulations. For permanent changes in ω^+ to occur here, transient GW-induced modifications to the tide must feed back to "self-accelerate" later portions of the wave packet that propagate into this region. Figures 3a, 3b, and 4b show that asymmetric $\mathcal{U}'_{\mathrm{TIDE}}$, $\partial\mathcal{U}'_{\mathrm{TIDE}}/\partial z$, and $\partial\mathcal{U}'_{TIDE}/\partial t$ profiles arise from transient forcing by a single wave. On substituting these terms into (1) and (2) we see that subsequent packets which propagate through the modified

wind profile $\mathcal{U}'_{\text{TIDE}}$ can undergo small net changes in m and ω and hence ω^+ on propagating through one full tidal cycle. If ω^+ increases (decreases), wave packets which propagate through $\mathcal{U}'_{\text{TIDE}}$ gain (lose) energy during the interaction and thus attenuate (amplify) the tide [e.g., *Broutman and Grimshaw*, 1988].

These arguments, however, ignore saturation and a host of other possible nonlinear influences. To assess these effects, a more complete numerical model is required which incorporates finite-amplitude wave mean-flow interactions. The next logical extension from here would probably be a "quasi-linear" numerical model of gravity wave self-acceleration and saturation processes within tidal profiles, following similar models of these processes within mean flows [e.g., *Jones and Houghton*, 1971, 1972; *Dunkerton and Fritts*, 1984; *Mobbs*, 1985; *Tanaka*, 1986; *Tanaka and Yoshizawa*, 1987]. However, comprehensive nonlinear models of transient gravity wave mean-flow interactions have suggested that certain aspects of the evolution are intrinsically nonlinear and thus beyond the scope of any slowly varying small-amplitude quasi-linear model [*Fritts and Dunkerton*, 1984; *Walterscheid and Schubert*, 1990; *Fritts et al.*, 1996]. Thus nonlinear modeling approaches may ultimately be needed to specify fully the role of gravity wave transience in GW-tidal interactions. Since tides are just large-scale gravity waves, this work may also aid modeling of GW-GW interactions involving a big wave and short wave, which are believed to be important in the formation of atmospheric GW spectra [*Hines*, 1991].

Of further interest were the numerical simulations in Figure 7 which showed that the interaction of a train of initially steady monochromatic plane-parallel gravity waves with an isolated tidal structure could induce permanent $\partial(kA)/\partial t$ variations in the emergent wave field. It was noted that at higher altitudes, wave dissipation at "focusing phases" could force a disturbance with a similar tidal period but that it would probably propagate downward. These findings raise some interesting questions concerning diurnally varying gravity wave activity and its possible influence on tides in the middle and upper atmosphere.

It has been argued that diurnal variability in tropical convective zones provides a strong thermal forcing of tidal modes [e.g., *Lindzen*, 1978; *Hamilton*, 1981; *Williams and Avery*, 1996]. *Bergman and Salby* [1994] found that direct convective forcing of planetary-scale tides was limited; it tended to force diurnal oscillations over a broad range of spatial scales. They also inferred strong gravity wave EP flux production by convection. Observations have also indicated that diurnally varying convection produces a diurnal variation in the intensity of convectively generated high-frequency gravity waves entering the middle atmosphere [e.g., *Nastrom and Eaton*, 1995; *Sato et al.*, 1995]. This implies a diurnally varying $\partial(kA)/\partial t$ for gravity waves produced by convective sources in the lower atmosphere. Depending on its phase relationship with existing tidal accelerations $\partial U'_{\text{TIDE}}/\partial t$, such diurnal $\partial(kA)/\partial t$ values will either amplify or attenuate tides in the middle atmosphere, according to (26) and (28), and might provide an indirect route for convective tidal forcing.

Summary and Conclusions

Ray simulations of gravity wave propagation through an idealized tidal background have shown that tidal accelerations modify not only ray paths, as was shown by *Zhong et al.* [1995], but also gravity wave amplitudes. When compared to a Lindzen parameterization of these dynamics, substantially altered predictions about both the locations and amounts of gravity wave breaking within the tide result. We demonstrated that correcting the ray path (thus including c_x variations) without correcting the wave amplitude brings the calculations closer to the full ray solution. Consequently, we proposed an adapted Lindzen parameterization, which incorporated c_x variations but retained its original nontransient wave-amplitude formulae, for use in improved modeling of GW-tidal interactions and perhaps other GW interactions with a time-evolving background.

Even in the absence of wave breaking, our amplitude calculations (based on wave-action conservation) revealed that time-varying gravity wave EP flux divergences resulted from tidal refraction and, consequently, were highly phase coherent with the tidal oscillation. Elementary analysis showed that a temporary increase in the amplitude of the tidal velocity oscillation resulted and that permanent energy transfers between the tide and gravity wave might occur in a more complete interactive simulation of these processes. As some initial observational support for the transient GW amplitudes that we simulated, we demonstrated characteristic anticorrelations between tidal velocity oscillations and gravity wave pseudomomentum flux densities in agreement with observations. In short, our simulations have stressed the importance of tidal time oscillations in obtaining an accurate description of GW-tidal interactions.

Appendix A: Numerical Ray-Tracing Solution of the Wave-Action Equation

In the first version of GROGRAT [*Marks and Eckermann*, 1995], possible time variations in the model atmosphere were not included. Thus $\partial c_{gz}/\partial t = 0$, where $c_{gz} = dz/dt$ is the ground-based vertical group velocity of the wave, which then enabled the wave-action continuity equation (8) to be reexpressed as a pseudo-ray-tracing equation for $F = c_{gz}A$. Since time variations in the background atmosphere are included here, then $\partial c_{gz}/\partial t \neq 0$ and the current implementation of the wave-action equation is no longer valid. Here we present a numerical solution of the wave-action equation which is valid in atmospheres which vary in both height and time.

Our implementation is similar to that of *Broutman* [1984]. On ignoring background horizontal gradients and dissipative effects the wave-action equation can be expressed in the pseudo-ray-tracing form (9), i.e.,

$$\frac{dA}{dt} = -A\,\frac{\partial c_{gz}}{\partial z}. \tag{A1}$$

The form is "pseudo-ray tracing" because in general $\partial c_{gz}/\partial z$ cannot be evaluated using a single ray but instead requires simultaneous tracing of a "tube" of closely spaced rays of similar initial characteristics.

However, we can avoid ray tube calculations here on manipulating (A1). First, we express the dispersion relation (11) in the form

$$\omega(z, t) = \Upsilon(\boldsymbol{\kappa}, z, t), \tag{A2}$$

where $\boldsymbol{\kappa} = (k, l, m)$, $(\boldsymbol{\kappa}, z, t)$ is the so-called augmented space, and (z, t) is the propagation space [*Hayes*, 1970]. The ray equations follow from (A2) and yield [*Hayes*, 1970; *Whitham*, 1974]

$$c_{gz} = \partial \Upsilon / \partial m. \tag{A3}$$

Since $m = m(z, t)$, then (A2) and (A3) can be used to reexpress (A1) as

$$\frac{dA}{dt} = -A\left(\frac{\partial^2 \Upsilon}{\partial m^2}\frac{\partial m}{\partial z} + \frac{\partial^2 \Upsilon}{\partial z\, \partial m}\right). \tag{A4}$$

Since the mean vertical wind velocity $W = 0$ here, then using the relations of *Marks and Eckermann* [1995],

$$\frac{\partial^2 \Upsilon}{\partial m^2} = \frac{-(k^2 + l^2)(N^2 - f^2)}{\omega^{+}\Delta^2}\left[1 - \frac{m^2}{\Delta}\left(3 + \frac{f^2}{\omega^{+2}}\right)\right], \tag{A5}$$

$$\frac{\partial^2 \Upsilon}{\partial z\, \partial m} = \frac{-(k^2 + l^2)m}{\omega^{+}\Delta^2}\left[(N^2)_z - \frac{(N^2 - f^2)}{2\Delta} \cdot \left(3(\alpha^2)_z + \frac{(k^2 + l^2)(N^2)_z + f^2(\alpha^2)_z}{\omega^{+2}}\right)\right], \tag{A6}$$

where subscripted background atmospheric variables denote local partial derivatives of that parameter (i.e., derivatives in the propagation space).

We are now left with the problem of computing $\partial m/\partial z$ in (A4), which generally requires the ray tube calculation. An elegant way of calculating it within the backgrounds considered here is to use the "derived ray equations" of *Hayes* [1970], following *Broutman* [1984]. On taking $\partial/\partial z$ to both sides of the ray equation $dm/dt = -\partial \Upsilon/\partial z$ one obtains a ray-tracing equation for $\partial m/\partial z$, which, on substituting the expression for $\partial c_{gz}/\partial z$ from (A4), takes the form

$$\frac{d}{dt}\left(\frac{\partial m}{\partial z}\right) = -\left[\frac{\partial^2 \Upsilon}{\partial z^2} + 2\left(\frac{\partial m}{\partial z}\right)\frac{\partial^2 \Upsilon}{\partial z\, \partial m} + \left(\frac{\partial m}{\partial z}\right)^2 \frac{\partial^2 \Upsilon}{\partial m^2}\right], \tag{A7}$$

where

$$\frac{\partial^2 \Upsilon}{\partial z^2} = kU_{zz} + lV_{zz} + \frac{(k^2 + l^2)}{2\omega^{+}\Delta^2}\left\{(N^2)_{zz}\Delta - (\alpha^2)_{zz}(N^2 - f^2) - \left((N^2)_z - \frac{(\alpha^2)_z(N^2 - f^2)}{\Delta}\right) \cdot \left(\frac{(k^2 + l^2)(N^2)_z + (\alpha^2)_z f^2}{\omega^{+2}} + 3(\alpha^2)_z\right)\right\}. \tag{A8}$$

In the simulations conducted here, background gradients in V, N^2, and α^2 are ignored, whereupon (A6) is identically zero and the right-hand side of (A8) simplifies to kU_{zz}.

Thus $\partial m/\partial z$ can be evaluated along a ray by integrating (A7) in conjunction with the other ray equations. However, one still requires its initial value in order to do this. Approximations such as $\partial m/\partial z \approx c_{gz}^{-1} dm/dt$ are inadequate, as the wave-action density A, evaluated along the ray using (A4), proves acutely sensitive to even slight initial errors in $\partial m/\partial z$. For the simulations outlined in this paper the following approaches were adopted. For tides of constant amplitude, gravity waves were launched either at peaks or troughs of the tide for which $\partial m/\partial z = 0$ is an accurate initial condition when temperature and density gradients are ignored. For modulated tidal amplitudes we launch gravity waves of identical initial parameters at regularly spaced time intervals from a lower height where the tidal amplitude was very close to zero. On launching monochromatic waves, plane-parallel ray paths result (see Figure 7a) for which $\partial m/\partial z = 0$ initially.

The $\partial m/\partial z$ values are also used to check that the WKB approximation remains valid along the ray path, using (3). They can also be used to evaluate (5) through the relation

$$\frac{\partial \omega^{+}}{\partial t} = -kc_{gz}U_z - c_{gz}^2 \frac{\partial m}{\partial z} + \frac{1}{2\omega^{+}\Delta} \cdot [(N^2)_l(k^2 + l^2) - (\alpha^2)_l(\omega^{+2} - f^2)] - \frac{c_{gz}}{2\omega^{+}\Delta} \cdot [(N^2)_z(k^2 + l^2) - (\alpha^2)_z(\omega^{+2} - f^2)]. \tag{A9}$$

The above equation follows from first expanding $d\omega^{+}/dt$ using the definition $\omega^{+} = \omega - kU$ and then simplifying using the ray-tracing equations for ω and m, the phase consistency relation $\partial m/\partial t = -\partial \omega/\partial z$, and discarding horizontal-gradient terms (which also imply a constant k). A relation similar to (A9) was derived by *Broutman* [1984].

Appendix B: Time-Varying Phase Speeds Within a Lindzen Parameterization

Here we briefly describe a method whereby time-varying c_x values can be incorporated into GW-drag parameterizations based on the *Lindzen* [1981] formulation. These changes have not been tested in a large-scale model, so there may be better ways of coding these effects operationally.

We envisage an array of ground-based horizontal phase speeds $c_{i,j,n}$, where i and j are array indices at model points along the x and y directions, respectively, and n is the "nth" ray at this horizontal location (i, j). In common with many implementations of the Lindzen parameterization we ignore oblique wave propagation paths and consider only the vertical wave propagation above the starting horizontal location (i, j). The current height of the various waves is stored in an array $z_{i,j,n}$.

In the Lindzen parameterization, c_x values are constant, whereas here we allow them to change in response to time-varying background conditions. If we assume that all of these waves have the same (constant) zonally aligned horizontal wavenumber k, then $\omega^{+}_{i,j,n} = k(c_{i,j,n} - \bar{U})$ and $m_{i,j,n}$ is given by the dispersion relation, where the background zonal wind speed $\bar{U}$ is evaluated at the wave's current location (as given by i, j, and $z_{i,j,n}$) and at the current time t.

Before going on to the next time step of a model run we evaluate dm/dt for each $m_{i,j,n}$ value using (1), again at the position $(i, j, z_{i,j,n})$ that the wave now occupies. Since most implementations of the Lindzen parameterization are hydrostatic and use zonally aligned waves, only the first and third terms on the right of (1) are needed. The third term could easily be omitted too, since its effects are generally small. If retained, the third term should be simplified to reflect a hydrostatic dispersion relation.

If the model time step is Δt, then $m_{i,j,n}$ is incremented by an amount $\Delta t(dm_{i,j,n}/dt)$. Next we evaluate $\omega^{+}_{i,j,n}$ for each ray using the (hydrostatic) dispersion relation. We can then update the phase speed values as $c_{i,j,n} = \omega^{+}_{i,j,n}/k + \bar{U}$. Finally, we use these new parameters to propagate the wave packet to its new height by incrementing $z_{i,j,n}$ by $\Delta t(c_{gz})_{i,j,n}$.

These updated parameters can then be used to quantify the GW-drag on the atmosphere at the next time step of the model using the formulae of the Lindzen parameterization (some

vertical interpolation may be required to regrid the results at the irregularly spaced heights $z_{i,j,n}$ onto the regular height grid of the model). If time and height variations of the background atmosphere are present and horizontal variations are small, then $c_{i,j,n}$ will now vary implicitly according to (2). One could also integrate (2) explicitly for each wave as a check of the numerics.

In simulations of GW-tidal interactions these modifications should be fairly robust, as illustrated in Figure 8. The exact response of a complex circulation model to this modified parameterization is harder to gauge. For example, one clear side effect is that gravity wave drag itself drives $\partial \bar{U}/\partial t$ variations, which will then feed back via (2) to accelerate the original $c_{i,j,n}$ values of the gravity waves. However, such "self-acceleration" effects have been observed in model simulations and may be a real feature of the gravity-wave driving. WKB methods such as these are incapable of fully simulating all aspects of these interactions [*Fritts and Dunkerton*, 1984; *Mobbs*, 1987; *Walterscheid and Schubert*, 1990; *Fritts et al.*, 1996], but could they simulate the first-order effects?

To investigate this, we look to the results of numerical models. Perhaps the most detailed study to date of gravity wave dissipation and self-acceleration within evolving mean flows was reported by *Walterscheid and Schubert* [1990], based on experiments with a nonlinear two-dimensional numerical model. They found that dissipating gravity waves which accelerated the background flow tended to self-accelerate in a way that kept their intrinsic phase speeds approximately constant with height, a process they were unable to explain.

Ray theory seems to provide a simple explanation of this feature. In the model runs of *Walterscheid and Schubert* [1990], $\partial \bar{U}/\partial z$ was generally small, but $\partial \bar{U}/\partial t$ was large and positive due to strong mean-flow accelerations induced by breaking gravity wave packets [see *Walterscheid and Schubert*, 1990, Figure 4]. As successive wave packets propagate into these regions of accelerating wind, if spatial wind gradients are small but $\partial \bar{U}/\partial t$ is large and is accelerating $\bar{U}$ toward the ground-based phase speed of the wave (as is typical of gravity-wave-induced mean-flow driving), then m remains approximately constant from (1) and ω refracts according to (2) to keep ω^+ approximately constant along the ray [e.g., *Jones*, 1969]. Since k also remains constant if horizontal gradients of the background wind are small, then constant ω^+ implies an approximately constant intrinsic phase speed $|c_x - \bar{U}|$, as found by *Walterscheid and Schubert* [1990].

From this it seems possible that a modified Lindzen parameterization which permits self-accelerated c_x values might even improve its simulation of mean-flow driving processes. Whether in practice self-accelerated c_x values improve or degrade the stability and/or performance of the parameterization in a larger-scale model remains to be seen. Of the existing GW-drag specifications the models of *Tanaka* [1986] and *Tanaka and Yoshizawa* [1987] have most in common with the modified Lindzen parameterization described here and produced mean circulations which were stable and basically in line with observations.

Acknowledgments. Thanks to Mary Anderson at Computational Physics, Inc., for her administrative support and to Joan Alexander and Dave Broutman for helpful comments on the manuscript.

References

Andrews, D. G., On the mean motion induced by transient inertio-gravity waves, *Pure Appl. Geophys.*, *118*, 177–188, 1980.

Andrews, D. G., and M. E. McIntyre, Planetary waves in horizontal and vertical shear: The generalized Eliassen-Palm relation and the mean zonal acceleration, *J. Atmos. Sci.*, *33*, 2031–2048, 1976.

Bacmeister, J. T., P. A. Newman, B. L. Gary, and K. R. Chan, An algorithm for forecasting mountain wave-related turbulence in the stratosphere, *Weather Forecasting*, *9*, 241–253, 1994.

Bergman, J. W., and M. L. Salby, Equatorial wave activity derived from fluctuations in observed convection, *J. Atmos. Sci.*, *51*, 3791–3806, 1994.

Bjarnason, G. G., S. Solomon, and R. R. Garcia, Tidal influences on vertical diffusion and diurnal variability of ozone in the mesosphere, *J. Geophys. Res.*, *92*, 5609–5620, 1987.

Blumen, W., Reflection of hydrostatic gravity waves in a stratified shear flow, I, Theory, *J. Atmos. Sci.*, *42*, 2255–2263, 1985.

Bretherton, F. P., and C. J. R. Garrett, Wavetrains in inhomogeneous moving media, *Proc. R. Soc. London A*, *302*, 529–554, 1969.

Broutman, D., The focusing of short internal waves by an inertial wave, *Geophys. Astrophys. Fluid Dyn.*, *30*, 199–225, 1984.

Broutman, D., On internal wave caustics, *J. Phys. Oceanogr.*, *16*, 1625–1635, 1986.

Broutman, D., and R. Grimshaw, The energetics of the interaction between short small-amplitude internal waves and inertial waves, *J. Fluid Mech.*, *196*, 93–106, 1988.

Broutman, D., and W. R. Young, On the interaction of small-scale internal waves with near-inertial waves, *J. Fluid Mech.*, *166*, 341–358, 1986.

Bruhwiler, D. L., and T. J. Kaper, Wavenumber transport: Scattering of small-scale internal waves by large-scale wavepackets, *J. Fluid Mech.*, *289*, 379–405, 1995.

Chao, W. C., and M. R. Schoeberl, On the linear approximation of gravity wave saturation in the mesosphere, *J. Atmos. Sci.*, *41*, 1893–1898, 1984.

Coy, L., and D. C. Fritts, Gravity wave heat fluxes: A Lagrangian approach, *J. Atmos. Sci.*, *45*, 1770–1780, 1988.

Coy, L., and M. Hitchman, Kelvin wave packets and flow accelerations: A comparison of modeling and observations, *J. Atmos. Sci.*, *41*, 1875–1880, 1984.

Dunkerton, T. J., Wave transience in a compressible atmosphere, I, Transient internal wave, mean-flow interaction, *J. Atmos. Sci.*, *38*, 281–297, 1981.

Dunkerton, T. J., Inertia-gravity waves in the stratosphere, *J. Atmos. Sci.*, *41*, 3396–3404, 1984.

Dunkerton, T. J., and D. C. Fritts, Transient gravity wave-critical layer interaction, I, Convective adjustment and the mean zonal acceleration, *J. Atmos. Sci.*, *41*, 992–1007, 1984.

Einaudi, F., and C. O. Hines, WKB approximation in application to acoustic-gravity waves, *Can. J. Phys.*, *48*, 1458–1471, 1970.

Eliassen, A., and E. Palm, On the transfer of energy in stationary mountain waves, *Geophys. Norr.*, *22*(3), 1–23, 1960.

Forbes, J. M., J. Gu, and S. Miyahara, On the interactions between gravity waves and the propagating diurnal tide, *Planet. Space Sci.*, *39*, 1249–1257, 1991.

Fritts, D. C., A numerical study of gravity wave saturation: Nonlinear and multiple wave effects, *J. Atmos. Sci.*, *42*, 2043–2058, 1985.

Fritts, D. C., Gravity wave-tidal interactions in the middle atmosphere: Observations and theory, in *The Upper Mesosphere and Lower Thermosphere: A Review of Experiment and Theory*, *Geophys. Monogr. Ser.*, vol. 87, edited by R. M. Johnson and T. L. Killeen, pp. 121–131, AGU, Washington, D. C., 1995.

Fritts, D. C., and T. J. Dunkerton, A quasi-linear study of gravity-wave saturation and self acceleration, *J. Atmos. Sci.*, *41*, 3272–3289, 1984.

Fritts, D. C., and W. Lu, Spectral estimates of gravity wave energy and momentum fluxes, II, Parameterization of wave forcing and variability, *J. Atmos. Sci.*, *50*, 3695–3713, 1993.

Fritts, D. C., and R. A. Vincent, Mesospheric momentum flux studies at Adelaide, Australia: Observations and a gravity wave/tidal interaction model, *J. Atmos. Sci.*, *44*, 605–619, 1987.

Fritts, D. C., S. A. Smith, B. B. Balsley, and C. R. Philbrick, Evidence of gravity wave saturation and local turbulence production in the summer mesosphere and lower thermosphere during the STATE experiment, *J. Geophys. Res.*, *93*, 7015–7025, 1988.

Fritts, D. C., J. F. Garten, and Ø. Andreassen, Wave breaking and

transition to turbulence in stratified shear flows, *J. Atmos. Sci., 53*, 1057–1085, 1996.

Ganguly, S., Incoherent scatter observations of mesospheric dynamics at Arecibo, *Geophys. Res. Lett., 7*, 369–372, 1980.

Garcia, R. R., and B. A. Boville, "Downward control" of the mean meridional circulation and temperature distribution of the polar winter stratosphere, *J. Atmos. Sci., 51*, 2238–2245, 1994.

Garcia, R. R., and S. Solomon, The effect of breaking gravity waves on the dynamics and chemical composition of the mesosphere and lower thermosphere, *J. Geophys. Res., 90*, 3850–3868, 1985.

Grimshaw, R., Wave action and wave-mean flow interaction, with applications to stratified shear flows, *Annu. Rev. Fluid Mech., 16*, 11–44, 1984.

Hamilton, K., Latent heat release as a possible forcing mechanism for atmospheric tides, *Mon. Weather Rev., 109*, 3–17, 1981.

Hamilton, K., Aspects of mesospheric simulation in a comprehensive general circulation model, in *The Upper Mesosphere and Lower Thermosphere: A Review of Experiment and Theory, Geophys. Monogr. Ser.*, vol. 87, edited by R. M. Johnson and T. L. Killeen, pp. 255–264, AGU, Washington, D. C., 1995.

Hayes, W. D., Kinematic wave theory, *Proc. R. Soc. London A, 320*, 209–226, 1970.

Haynes, P. H., Forced, dissipative generalizations of finite-amplitude wave-activity conservation relations for zonal and nonzonal basic flows, *J. Atmos. Sci., 45*, 2352–2362, 1988.

Hines, C. O., The saturation of gravity waves in the middle atmosphere, II, Development of Doppler-spread theory, *J. Atmos. Sci., 48*, 1360–1379, 1991.

Holton, J. R., The generation of mesospheric planetary waves by zonally asymmetric gravity wave breaking, *J. Atmos. Sci., 41*, 3427–3430, 1984.

Huang, T. Y. W., and A. K. Smith, Dynamical and chemical feedback in a two-dimensional interactive model of the middle atmosphere, *J. Geophys. Res., 100*, 11,085–11,104, 1995.

Hunt, B. G., The impact of gravity wave drag and diurnal variability on the general circulation of the middle atmosphere, *J. Meteorol. Soc. Jpn., 64*, 1–16, 1986.

Hunt, B. G., A simulation of gravity wave characteristics and interactions in a diurnally varying model atmosphere, *J. Meteorol. Soc. Jpn., 68*, 145–161, 1990.

Jackson, D. R., and L. J. Gray, Simulation of the semi-annual oscillation of the equatorial middle atmosphere using the Extended UGAMP General Circulation Model, *Q. J. R. Meteorol. Soc., 120*, 1559–1588, 1994.

Jones, W. L., Ray tracing for internal gravity waves, *J. Geophys. Res., 74*, 2028–2033, 1969.

Jones, W. L., and D. D. Houghton, The coupling of momentum between gravity waves and mean flow: A numerical study, *J. Atmos. Sci., 28*, 604–608, 1971.

Jones, W. L., and D. D. Houghton, The self-destructing internal gravity wave, *J. Atmos. Sci., 29*, 844–849, 1972.

Keller, T. L., Implications of the hydrostatic approximation on atmospheric gravity waves, *J. Atmos. Sci., 51*, 1915–1929, 1994.

Kinnersley, J. S., The climatology of the stratospheric "THIN AIR" model, *Q. J. R. Meteorol. Soc., 122*, 219–252, 1996.

Laprise, J. P. R., An assessment of the WKBJ approximation to the vertical structure of linear mountain waves: Implications for gravity-wave drag parameterization, *J. Atmos. Sci., 50*, 1469–1487, 1993.

Lindzen, R. S., Effect of daily variations in cumulonimbus activity on the atmospheric semidiurnal tide, *Mon. Weather Rev., 106*, 526–533, 1978.

Lindzen, R. S., Turbulence and stress owing to gravity wave and tidal breakdown, *J. Geophys. Res., 86*, 9707–9714, 1981.

Lindzen, R. S., Gravity waves in the mesosphere, in *Dynamics of the Middle Atmosphere*, edited by J. R. Holton and T. Matsuno, pp. 3–18, Terrapub, Tokyo, 1984.

Lindzen, R. S., Supersaturation of vertically propagating internal gravity waves, *J. Atmos. Sci., 45*, 705–711, 1988.

Lu, W., and D. C. Fritts, Spectral estimates of gravity wave energy and momentum fluxes, III, Gravity wave–tidal interactions, *J. Atmos. Sci., 50*, 3714–3727, 1993.

Manson, A. H., C. E. Meek, H. Teitelbaum, F. Vial, R. Schminder, D. Kürschner, M. J. Smith, G. J. Fraser, and R. R. Clark, Climatologies of the semi-diurnal and diurnal tides in the middle atmosphere (70–110 km) at middle latitudes (40–55°), *J. Atmos. Terr. Phys., 51*, 579–593, 1989.

Marks, C. J., and S. D. Eckermann, A three-dimensional nonhydrostatic ray-tracing model for gravity waves: Formulation and preliminary results for the middle atmosphere, *J. Atmos. Sci., 52*, 1959–1984, 1995.

McIntyre, M. E., On dynamics and transport near the polar mesopause in summer, *J. Geophys. Res., 94*, 14,617–14,628, 1989.

McLandress, C., and W. E. Ward, Tidal/gravity wave interactions and their influence on the large-scale dynamics of the middle atmosphere: Model results, *J. Geophys. Res., 99*, 8139–8155, 1994.

McLandress, C., G. G. Shepherd, and B. H. Solheim, Satellite observations of thermospheric tides: Results from the Wind Imaging Interferometer on UARS, *J. Geophys. Res., 101*, 4093–4114, 1996.

Medvedev, A. S., and G. P. Klaassen, Vertical evolution of gravity wave spectra and the parameterization of associated wave drag, *J. Geophys. Res., 100*, 25,841–25,853, 1995.

Miyahara, S., Suppression of stationary planetary waves by internal gravity waves in the mesosphere, *J. Atmos. Sci., 42*, 100–107, 1985.

Miyahara, S., and J. M. Forbes, Interactions between diurnal tides and gravity waves in the lower thermosphere, *J. Atmos. Terr. Phys., 56*, 1365–1373, 1994.

Miyahara, S., Y. Hayashi, and J. D. Mahlmann, Interactions between gravity waves and planetary-scale flow simulated by the GFDL "SKYHI" general circulation model, *J. Atmos. Sci., 43*, 1844–1861, 1986.

Miyahara, S., Y. Yoshida, and Y. Miyoshi, Dynamic coupling between the lower and upper atmosphere by tides and gravity waves, *J. Atmos. Terr. Phys., 55*, 1039–1053, 1993.

Mobbs, S. D., Propagation of nonlinear internal gravity waves at stratospheric and mesospheric heights, II, Solutions for model atmospheres, *Ann. Geophys., Ser. A, 3*, 451–464, 1985.

Mobbs, S. D., A numerical investigation of nonlinear internal gravity waves and their influence on the mean flow, *Ann. Geophys., Ser A, 5*, 197–208, 1987.

Nastrom, G. D., and F. D. Eaton, Variations of winds and turbulence seen by the 50-MHz radar at White Sands Missile Range, New Mexico, *J. Appl. Meteorol., 34*, 2135–2148, 1995.

Palmer, T. N., G. J. Shutts, and R. Swinbank, Alleviation of a systematic westerly bias in general circulation and numerical weather prediction models through an orographic gravity wave drag parameterization, *Q. J. R. Meteorol. Soc., 112*, 1001–1040, 1986.

Roble, R. G., and E. C. Ridley, A thermosphere-ionosphere-mesosphere-electrodynamics general circulation model (time-GCM): Equinox solar cycle minimum simulations (30–500 km), *Geophys. Res. Lett., 21*, 417–420, 1994.

Sato, K., H. Hashiguchi, and S. Fukao, Gravity waves and turbulence associated with cumulus convection observed with the UHF/VHF clear-air Doppler radars, *J. Geophys. Res., 100*, 7111–7119, 1995.

Schoeberl, M. R., A ray tracing model of gravity wave propagation and breakdown in the middle atmosphere, *J. Geophys. Res., 90*, 7999–8010, 1985.

Schoeberl, M. R., and D. F. Strobel, Nonzonal gravity wave breaking in the winter stratosphere, in *Proceedings of the U.S.-Japan Seminar on Dynamics of the Middle Atmosphere*, edited by J. R. Holton and T. Matsuno, pp. 45–64, Terrapub, Tokyo, 1984.

Scinocca, J. F., and T. G. Shepherd, Nonlinear wave-activity conservation laws and Hamiltonian structure for the two-dimensional anelastic equations, *J. Atmos. Sci., 49*, 5–27, 1992.

Smith, A. K., Longitudinal variations in mesospheric winds: Evidence for gravity wave filtering by planetary waves, *J. Atmos. Sci., 53*, 1156–1173, 1996.

Spizzichino, A., Study of the interactions between the different components of the wind in the high atmosphere, 4, Study of the interaction between the diurnal tide and gravity waves, *Ann. Geophys., 26*, 9–24, 1970.

Tanaka, H., A slowly varying model of the lower stratospheric zonal wind minimum induced by mesoscale mountain wave breakdown, *J. Atmos. Sci., 43*, 1881–1892, 1986.

Tanaka, H., and N. Yoshizawa, A slowly varying model of the quasi-biennial oscillation involving effects of transience, self-acceleration and saturation of equatorial waves, *J. Atmos. Sci., 44*, 1427–1436, 1987.

Thayaparan, T., W. K. Hocking, and J. MacDougall, Observational evidence of tidal/gravity wave interactions using the UWO 2 MHz radar, *Geophys. Res. Lett., 22*, 373–376, 1995.

Thorpe, S. A., The distortion of short internal waves produced by a

long wave, with application to ocean boundary mixing, *J. Fluid Mech.*, *208*, 395–415, 1989.

Vincent, R. A., T. Tsuda, and S. Kato, A comparitive study of mesospheric solar tides observed at Adelaide and Kyoto, *J. Geophys. Res.*, *93*, 699–708, 1988.

Walterscheid, R. L., Inertio-gravity wave induced accelerations of mean flow having an imposed periodic component: Implications for tidal observations in the meteor region, *J. Geophys. Res.*, *86*, 9698–9706, 1981.

Walterscheid, R. L., Gravity wave mean state interactions in the upper mesosphere and lower thermosphere, in *The Upper Mesosphere and Lower Thermosphere: A Review of Experiment and Theory*, *Geophys. Monogr. Ser.*, vol. 87, edited by R. M. Johnson and T. L. Killeen, pp. 133–144, AGU, Washington, D. C., 1995.

Walterscheid, R. L., and G. Schubert, Nonlinear evolution of an upward propagating gravity wave: Overturning, convection, transience, and turbulence, *J. Atmos. Sci.*, *47*, 101–125, 1990.

Wang, D.-Y., and D. C. Fritts, Evidence of gravity wave-tidal interaction observed near the summer mesopause at Poker Flat, Alaska, *J. Atmos. Sci.*, *48*, 572–583, 1991.

Whitham, G. B., *Linear and Non-linear Waves*, 636 pp., Academic, San Diego, Calif., 1974.

Williams, C. R., and S. K. Avery, Diurnal nonmigrating tidal oscillations forced by deep convective clouds, *J. Geophys. Res.*, *101*, 4079–4091, 1996.

Yamamoto, M., T. Tsuda, S. Kato, T. Sato, and S. Fukao, A saturated inertia gravity wave in the mesosphere observed by the middle and upper atmosphere radar, *J. Geophys. Res.*, *92*, 11,993–11,999, 1987.

Zhong, L., L. J. Somnor, A. H. Manson, and C. E. Meek, The influence of time-dependent wind on gravity-wave propagation in the middle atmosphere, *Ann. Geophys.*, *13*, 375–394, 1995.

S. D. Eckermann, E. O. Hulburt Center for Space Research, Code 7641, Naval Research Laboratory, Washington, D. C. 20375. (e-mail: eckerman@ismap4.nrl.navy.mil)

C. J. Marks, National Institute of Water and Atmospheric Research Limited, 310 Evans Bay Parade, Box 14901, Wellington, New Zealand. (e-mail: marks@thor.niwa.cri.nz)

(Received October 27, 1995; revised May 16, 1996; accepted May 16, 1996.)